Journal of Asian Earth Sciences 229 (2022) 105149

Contents lists available at ScienceDirect

Journal of Asian Earth Sciences

journal homepage: www.elsevier.com/locate/jseaes

The thermal history in sedimentary basins: A case study of the central Tarim Basin, Western China

Dan Li [a,b], Jian Chang [a,b,*], Nansheng Qiu [a,b], Jiangshan Wang [a,b], Mengran Zhang [a,b], Xian Wu [c], Jun Han [c], Huili Li [d], Anlai Ma [d]

[a] State Key Laboratory of Petroleum Resources and Prospecting, China University of Petroleum, Beijing 102249, China
[b] Basin and Reservoir Research Center, China University of Petroleum, Beijing 102249, China
[c] Exploration and Production Research Institute of Northwest Oilfield Branch, SINOPEC, Urumqi, Xinjiang 830011, China
[d] Sinopec Petroleum Exploration & Production Research Institute, Beijing 100083, China

ARTICLE INFO

Keywords:
Tarim Basin
Northern Shuntuoguole area
Thermal history
Hydrocarbon charging
Equivalent vitrinite reflectance
Fluid inclusion

ABSTRACT

The reconstruction of thermal history is essential for the superdeep (>6,000 m) hydrocarbon exploration and development in the Central Tarim Basin, Western China. This study first recovered the burial histories of five typical wells in the Shunbei area (the Central Tarim Basin) based on the drilling data and calculated the erosional thicknesses using the well-tie profiles. The thermal histories and hydrocarbon charging periods of the Shunbei area were studied with the measured equivalent vitrinite reflectance (R_{equ}) and fluid inclusion assemblage homogenization temperature data, respectively. Except for some abnormal values, most R_{equ} data with 0.45%–1.48% gradually increase with depth. The thermal modeling revealed that the heat flow in the Shunbei area gradually decreased since the Early Ordovician, with an abrupt peak of ~45–47 mW/m^2 during the Early Permian. The temperature histories of the Ordovician Yijianfang and Yingshan Formation reservoirs in the Shunbei area could be divided into three stages of rapid heating (1.27–1.36 °C/Ma), slow heating (0.07–0.09 °C/Ma) and rapid heating (1.20–1.28 °C/Ma). We recognized three hydrocarbon charging periods in the No. 1 strike-slip fault zone, which occurred at ~435–420 Ma, ~263–220 Ma, and 18–3 Ma, respectively, while the No. 5 and 7 strike-slip fault zones only experienced the first two periods. This study provides new insights into the thermal history and hydrocarbon accumulation in the Shunbei area, which would be very useful for further superdeep oil and gas exploration and resource evaluation in the Central Tarim Basin.

1. Introduction

The superdeep strata with the depths > 6,000 m in the sedimentary basins become essential targets in hydrocarbon exploration and development along with the energy demand increase and more difficulty for finding new large oil fields in the shallow strata (Dyman et al., 2002; Jin, 2011; Sun et al., 2013; Jia and Pang, 2015; Zhu et al., 2018, 2019). Jia and Pang (2015) considered that ~40% of the total proved oil and gas reserves in the world were distributed in the superdeep strata. In recent years, >90% of new proved oil and gas reserves in the Tarim Basin, Western China, come from the superdeep strata (Zhu et al., 2019). Compared to the shallow strata, the superdeep hydrocarbon exploration in sedimentary basins confronts some unique and unsolved problems, such as formation model and maturation evolution of superdeep source rocks, genesis mechanism and prediction of superdeep reservoirs, hydrocarbon accumulation and enrichment pattern in the superdeep strata, and occurrence phase of the superdeep hydrocarbon (Li et al., 2020). All of these scientific problems were related to the geothermal field of the superdeep strata.

The Tarim Basin recently draws attention to the discovery of the Shunbei (the northern Shuntuoguole Low Uplift) oil field characterized by light oil reservoirs at the depths of ~7,000–8,500 m (Jiao, 2018; Gu et al., 2020a, 2020b). It is noted that the hydrocarbon phase at such great depths with the formation temperature of 145.3–154.5 °C in the Shunbei area, the central Tarim Basin, conflicts with the traditional "oil window" theory (60–120 °C) (Tissot and Welte, 1978). Most studies have discussed the thermal history of the Bachu Uplift, Katake Uplift, Shaya Uplift, and Kongquehe Slope in the Tarim Basin with vitrinite reflectance (Qiu et al., 2010), fission track (Li et al., 2005; Chang et al., 2014, 2019), and (U-Th)/He data (Qiu et al., 2011; Chang and Qiu,

* Corresponding author at: State Key Laboratory of Petroleum Resources and Prospecting, China University of Petroleum, Beijing 102249, China.
E-mail address: changjian@cup.edu.cn (J. Chang).

https://doi.org/10.1016/j.jseaes.2022.105149
Received 1 July 2021; Received in revised form 11 February 2022; Accepted 12 February 2022
Available online 18 February 2022

2017). For the Shunbei area, Liu et al. (2020) just investigated the abnormally high temperature of 170–190 °C in the Early Permian with the clumped isotope data. Therefore, it is necessary to reveal the detailed thermal history of the Shunbei area for explaining the occurrence of the light oil reservoir below the depth of ~7,000 m.

This study first reconstructed the thermal history of the Shunbei area based on the erosional thicknesses of unconformities, the measured equivalent vitrinite reflectance (R_{equ}), and the present-day temperature field. Then we simulated the paleo-temperature history of Ordovician reservoirs and identified the hydrocarbon charging periods according to the homogenization temperature data of fluid inclusion assemblage. Finally, the potential source rocks and differential hydrocarbon

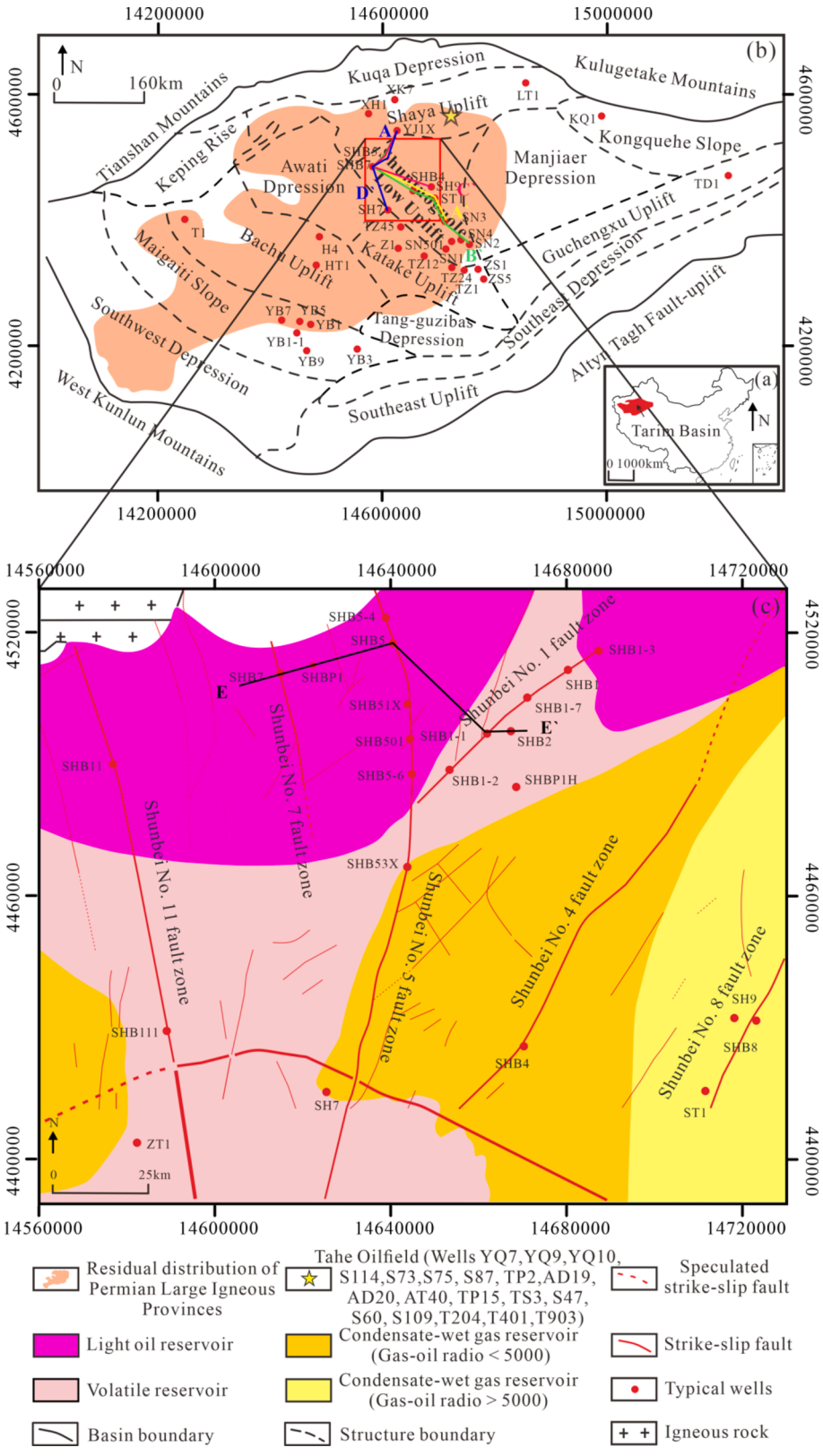

Fig. 1. (a) Tectonic framework of China indicates the Tarim Basin location. (b) Sketch of the tectonic units in Tarim Basin, showing locations of the studied area. Lines A–A', A–B', A–C', and A–D' represent the well-tie profiles shown in Figs. 4–9, respectively. Lines E–E' represents the profiles shown in Fig. 19. The distribution range of the Permian sizeable igneous province is drawn according to Yang et al. (2014). (c) Enlarged view of the studied area (Shunbei area), showing wells, strike-slip fault zones, and Ordovician reservoirs in the Shunbei area (modified from Qi, 2020).

accumulation in the Shunbei area and the Tarim Basin were discussed. This study not only indicates new insights into the thermal history of the Shunbei area since the Paleozoic, which are of significance for analyzing the oil and gas phase in the superdeep strata of the Tarim Basin, but also provides basic theory and research strategy for the superdeep thermal history analysis of the sedimentary basins in the world.

2. Geological setting

The Tarim Basin in western China is a typical multi-cycle superimposed basin, covering an area of 5.6 × 10^5 km^2. According to the characteristics of basement relief, stratigraphic sequence, and fault distribution, the platform-basin region of the Tarim Basin is divided into ten structural units: the Shuntuoguole Low Uplift, Shaya Uplift, Katake Uplift, Guchengxu Uplift, Bachu Uplift, Manjiaer Depression, Awati Depression, Tangguzibas Depression, Kongquehe Slope, and Maigaiti Slope (Fig. 1b; Ma et al., 2015). The Shuntuoguole Low Uplift bounds the Awati Depression to the west, the Manjiaer Depression to the east, the Shaya Uplift to the north, and the Katake Uplift to the south (Fig. 1b). The deep strata in the Shunbei area develop massive strike-slip fault zones, which act as the oil and gas migration pathways from the deep Cambrian and Ordovician source rocks to the shallow middle-lower Ordovician reservoirs (Fig. 1c; Lü et al., 2012; Zhu et al., 2017). The No. 1, 5, and 7 strike-slip fault zones in the Shunbei area play an important role in the regional transformation of the stress field. The western and eastern Shunbei areas, divided by the No. 5 strike-slip fault zone, are dominated by NW- and NE-striking fault systems, respectively (Fig. 1c; Lin et al., 2021).

The Tarim Basin, with an Archean and Proterozoic crystalline basement, is overlain by a Paleozoic marine craton basin and a Mesozoic–Cenozoic foreland basin (He et al., 2005; Zhang et al., 2013). During the Early Cambrian, the entire Tarim Basin was inundated by seawater due to global transgression (Yang et al., 2011; Li et al., 2015). The Shunbei area in the Central Tarim Basin evolved as a craton carbonate platform and deposited thick dolomite (Li et al., 2015). The Shunbei area then developed as semi-restricted and restricted platforms and deposited limestone and dolomite from the Late Cambrian to the Middle Ordovician (Chen et al., 2015). Due to the stress transition from extension to compression in the Late Ordovician, the Shunbei area experienced exhumation and generated several strike-slip fault zones, such as No. 1 and 5 strike-slip fault zones (Deng et al., 2018; Yang et al., 2020). The Shunbei area evolved as a coastal, shallow sea and dominantly deposited mudstone and sandstone during the Silurian (Zhang et al., 2008; Chang et al., 2012). The extensive tectonic movement in the Late Silurian caused the uplifting and erosion in the Tarim Basin, and the Shunbei area was lack of the top of the upper Silurian and the middle-lower Devonian (Fig. 2; Guo and Hong, 2007). Meanwhile, the inherited strike-slip fault zones developed across the Silurian strata (Jiao, 2018). During the Carboniferous, the Shunbei area evolved as an epicontinental marine environment and mainly deposited littoral and neritic clastic sediments (He et al., 2005). A large igneous province (PLIPs) formed with dramatic magmatic activity in the northwestern

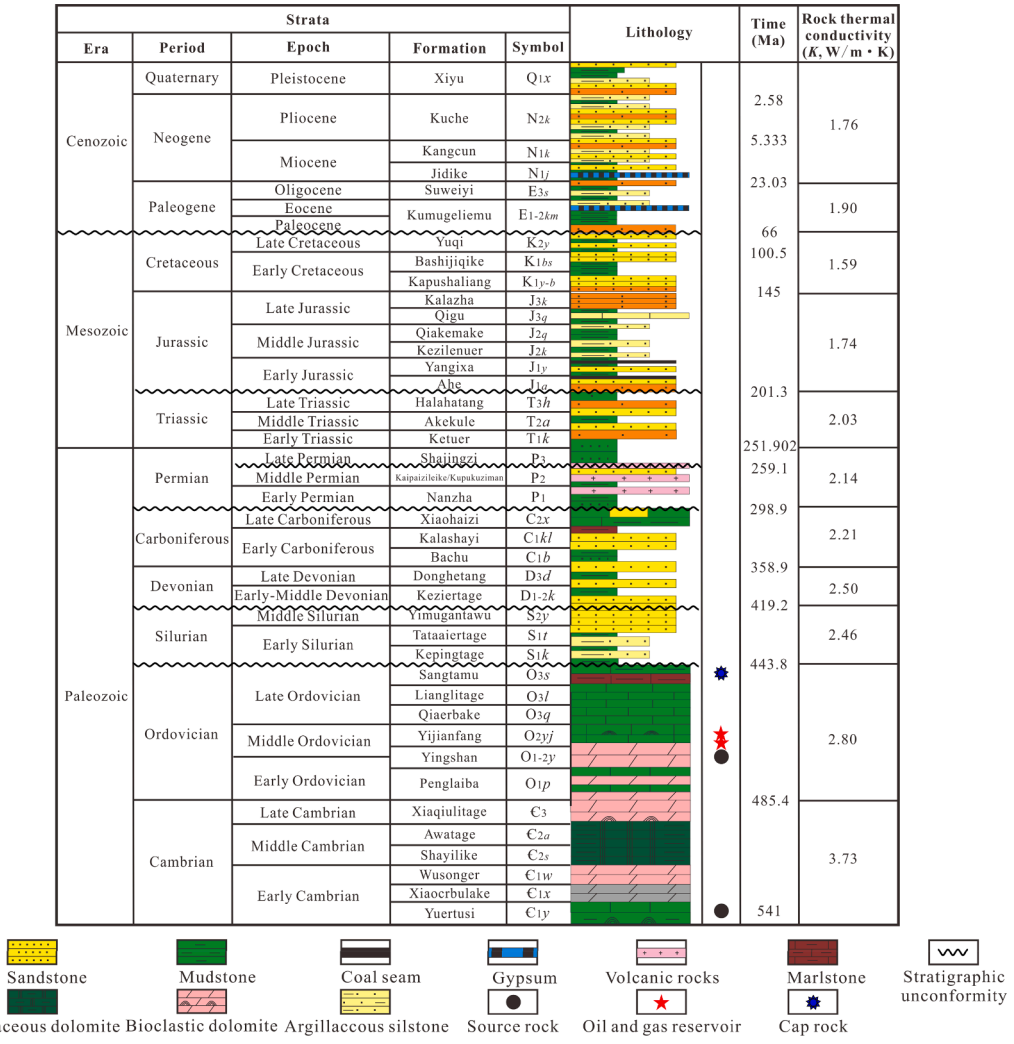

Fig. 2. General stratigraphic column of the Shunbei area, Tarim Basin (modified from Zhang et al., 2007). Thermal conductivity (*K*) data refer to Liu et al. (2015).

Tarim Basin during the Early Permian (Yang et al., 2014). It was mainly composed of basalt, diabase, and tuff with a maximum thickness of ~780 m (Fig. 2; Li et al. 2011, 2012a; Xu et al., 2014; Yang et al., 2014). With the closure of the South Tianshan Ocean, the Tarim Basin evolved from a marine basin to a fluvial continental lake basin in the Late Permian. Since the Mesozoic, the northern and southwestern margins of the Tarim Basin developed as a foreland basin. Due to the collision of the Tarim Plate with the Qiangtang Block, the Shunbei area experienced severe erosion from the Triassic to the Jurassic (Liu et al., 2020). Since the Cenozoic, the Shunbei area received massive clastic deposition with a thickness of ~2–3 km, along with the uplifting and erosion of the Tianshan (Fig. 2).

3. Thermal history reconstruction

3.1. Basic geological parameters

Wells SHB1, SHB2, SHB5, SHBP1, and ZT1 in the Shunbei area were selected for thermal history reconstruction based on the burial history, the vitrinite reflectance (R_o), and the present-day temperature field by the BasinMod 1-D software version 5.4 (Platte River Associates Inc., U. S., 2003). The present-day surface temperature was 14 °C for modeling purposes. The rock thermal conductivity and the present-day heat flow data refer to Liu et al. (2015) and Wu et al. (2022), respectively (Fig. 2; 32–42 mW/m^2). The burial histories of these wells were established based on the lithological data, stratigraphic data, and erosional thicknesses of unconformities. The lithological and stratigraphic data were obtained from the Exploration and Production Research Institute of the Northwest Oilfield Company, SINOPEC (Fig. 2 and Table 1). The calculated erosional thickness according to the well-tie profiles and the vitrinite reflectance is introduced in the next part.

3.2. Erosion thickness calculation

The Shunbei area in the central Tarim Basin experienced multiple tectonic uplift events, but the erosional thickness for each uplift event remains controversial (Lin et al., 2012; He et al., 2016; Qi, 2016; Jiao, 2018). As one depression area, the thickness of each stratum in the Shunbei area changes laterally with a certain degree of regularity. So, it is available to calculate the original stratal thickness before uplifting by using well-tie profiles based on the methods of nearby stratal thickness ratio (Equation (1); Fig. 3a) and stratal thickness change ratio (Equation (2); Fig. 3b), which were introduced in detail by Mu et al. (2002). For the nearly stratal thickness ratio method, the original stratal thickness was gotten from the well-preserved ratios of the stratal thickness of nearby and underlying layers in the well-tie profiles with poor stratigraphic

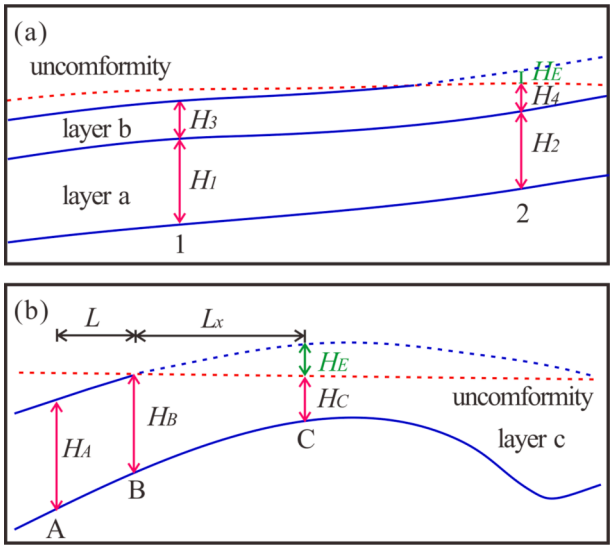

Fig. 3. Schematic diagram of calculating erosional thickness using the (a) Method of nearby stratal thickness ratio and (b) Method of stratal thickness change ratio (modified from Mu et al., 2002). H_E is the erosion thickness (m), H_1, H_2, H_3, H_A, and H_B are the original stratal thickness (m), H_4 and H_C are the residual stratal thickness (m), and L_x and L are the distances between the wells (m).

Table 1
The residual stratal thickness of the typical wells in the Shunbei area.

Formation	Symbol	Well SHB1		Well SHB2		Well SHB5		Well SHBP1		Well ZT1	
		Bottom depth (m)	Thickness (m)	Bottom depth (m)	Thickness (m)	Bottom depth (m)	Thickness (m)	Bottom depth (m)	Thickness (m)	Bottom depth (m)	Thickness (m)
Xiyu	Q_1x	78	78	79	79	86	86	80	80	300	300
Kuche	N_2k	1,909	1,831	1,902.5	1,823.5	2,226	2,140	2,164	2,084		
Kangcun	N_1k	2,503	594	2,497	594.5	2,912	686	2,776.5	612.5		
Jidike	N_1j	2,623	120	2,603	106	3,117	205	3,105	328.5	2,361	2,061
Suweiyi	E_3s	2,792	169	2,782	179	3,186	69	3,140	35		
Kumugeliemu	$E_{1-2}km$	2,805	13	2,797	15	3,198	12	3,161.5	21.5	2,772	711
Bashijiqike	K_1bs	3,297	492	3,232	435	3,646	448	3,612.5	451		
Kapushaliang	K_1y-b	3,708	411	3,615	383	4,024	378	3,992	379.5	3,096	324
Halahatang	T_3h	3,959	251	3,812	197	4,281	257	4,240.5	248.5		
Akekule	T_2a	4,413	454	4,292	480	4,711	430	4,630.5	390		
Ketuer	T_1k	4,529	116	4,422	130	4,786	75	4,743.5	113	4,066	970
Kaipaizileike–Kupukuziman	P_2	4,953	424	4,967	545	5,319	533	5,279	535.5	4,955	889
Xiaohaizi	C_2x									4,988	33
Kalashayi	C_1kl	5,132	179	5,139	172	5,415	96	5,407.5	128.5	5,126	138
Bachu	C_1b	5,281	149	5,299	160	5,581	166	5,552.5	145	5,412	286
Donghetang	D_3d	5,366	85	5,369	70	5,725	144	5,695	142.5	5,432	20
Keziertage	D_{1-2}k									5,638	206
Yimugantawu	S_2y									5,652	14
Tataaiertage	S_1t	6,099	733	6,115	746	6,348	623	6,450.5	755.5	6,130	478
Kepingtage	S_1k	6,453	354	6,510	395	6,804	456	6,788.5	338	6,526	396
Sangtamu	O_3s	7,259	806	7,326	816	7,294	490	7,520	731.5	7,101	575
Lianglitage	O_3l	7,262	3	7,336	10			7,531	11	7,186	85
Qiaerbake	O_3q	7,287	25	7,357	21	7,358	64	7,566	35		
Yijianfang	O_2yj	7,446	159	7,463.5	106.5	7,504	146	7,717	151		
Yingshan	$O_{1-2}y$			7,753.5	290	7,665	161				

continuity. In comparison, it is calculated based on the formation thickness change rate in the well-tie profiles with stratigraphic continuity for the stratal thickness change ratio method. The erosion thickness for each stratum was then calculated by the calculated original stratal thickness minus the residual stratal thickness.

$$H_E = H_2{}^*H_3/H_1 - H_4 \quad (1)$$

$$H_E = H_B + (H_B - H_A)\ {}^*L_X/L - H_C \quad (2)$$

Where H_1, H_2, H_3, H_A, and H_B are the original stratal thickness at points *1* and *2* of layer *a*, point *1* of layer *b*, points *A* and *B* of layer *c*, respectively; H_4 and H_C are the residual stratal thickness at point *2* of layer *b* and point *C* of layer *c*; H_E is the erosion thickness; *L* is the distance between points *A* and *B*; L_X is the distance between points *B* and *C*.

In this study, the nearby stratal thickness ratio method was used to calculate the erosional thicknesses during the Silurian and Carboniferous (Figs. 5 and 6), and the erosion thicknesses of the Ordovician, Permian, Triassic, and Cretaceous periods were calculated by the method of stratal thickness change ratio (Figs. 4, 7, 8 and 9). All the data for the calculated erosion thicknesses were summarized in Table 2. They were comparable with previous studies using other studied methods, including wave process analysis of sedimentary basin and paleotemperature scale methods (Qi and Liu, 1999; Zhang et al., 2000; Liu et al., 2020; Wang et al., 2020).

3.3. Equivalent vitrinite reflectance data

Vitrinite is a primary component of coals and other organic matter found in sedimentary rocks and used for reflectance measurements owing to its relatively progressive change in optical properties with increasing temperature (Tissot and Welte, 1978; Chang et al., 2017). Because the vitrinite does not exist in pre-Silurian rocks, the bitumen reflectance in the Ordovician sediments is measured to reconstruct the thermal history of the Shunbei area (Buchardt and Lewan, 1990). This experiment was carried out using a Leica DM4500P polarizing microscope (Leica Camera AG, Germany) with an MPS200 photometer (Monolithic Power Systems, America) at the Wuxi Institute of Petroleum Geology, Sinopec Petroleum Exploration & Production Research Institute, SINOPEC. Finally, the measured bitumen reflectance (R_b) data were converted into equivalent vitrinite reflectance (R_{equ}) data using the equations proposed by Wang et al. (1996) and Jacob (1989).

A dataset of 39 vitrinite or bitumen reflectance was measured for the samples of the Wells SHB1, SHB2, SHB5, SHBP1, and ZT1 with depths of 3,712–7,975 m (Fig. 10 and Table 3). Some measured R_{equ} data with (1.30%–4.85%) are abnormally larger in the lower Permian and Carboniferous of the Wells SHB1, SHB5, and ZT1 than a normal trend, probably related to the igneous activity that occurred in the Early Permian. Previous studies have demonstrated that the high temperature from the magma could enlarge the vitrinite reflectance in the sedimentary layers closed to the intrusive body (Fjeldskaar et al., 2008; Wang et al., 2011; Fig. 11). It is different from the intrusive rock in that the extrusive basalt in the Shunbei area just affected the thermal history of the underlying layers such as the lower Permian and Carboniferous (Fig. 10). Except for these abnormal R_{equ} data, other R_{equ} data range from 0.45% to 1.48%, showing a positive correlation with depth (Fig. 10 and Table 3).

3.4. Thermal history modeling

In this study, the R_{equ} data were used as a constraint to simulate the paleo-heat flow history of the Shunbei area based on the Easy% R_o model (Sweeney and Burnham, 1990). We first restored the typical wells' burial histories according to the drilling data and calculated erosional thicknesses. Then the measured R_{equ} data and the present-day heat flow were input as the constraints. Secondly, the paleo-heat flow paths were repeatedly changed as forward modeling for comparing the modeled R_{equ} paths with the measured R_{equ} data (Chang et al., 2018; Jiang et al., 2021). When the modeled R_{equ} paths are consistent with the measured R_{equ} data, the heat flow path at this time is considered to be the real paleo-heat flow evolution path. Finally, the paleo-heat flow histories of the Wells SHB1, SHB2, SHB5, SHBP1, and ZT1 were reconstructed based on the measured R_{equ} data (Fig. 12).

The paleo-heat flow in the Shunbei area gradually decreased since the Early Paleozoic was controlled by the tectonic evolution and superimposed the influences of regional tectonic-thermal events (Fig. 12f and Table 4). The Tarim Basin was a continental rift during the Cambrian–Early Ordovician (Lin et al., 2012). The stretching and thinning of the crust (Qiu et al., 2012) resulted in the heat flow values in the Early Ordovician being relatively high at ~39–44 mW/m^2. With the ocean basin closure around the Tarim plate during the Middle Ordovician–Devonian (Zhang et al., 2007), the Tarim Basin entered an

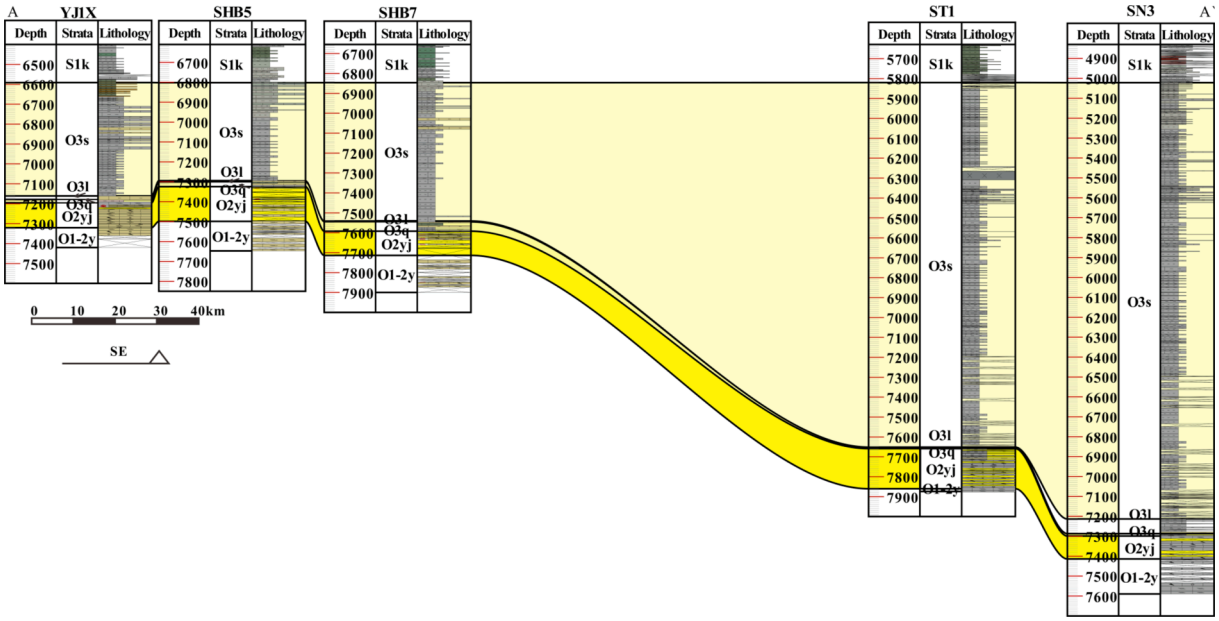

Fig. 4. Ordovician well-tie profile in the Shunbei area, Tarim Basin (Wells YJ1X, SHB5, SHB7, ST1, and SN3; location is shown in Fig. 1b).

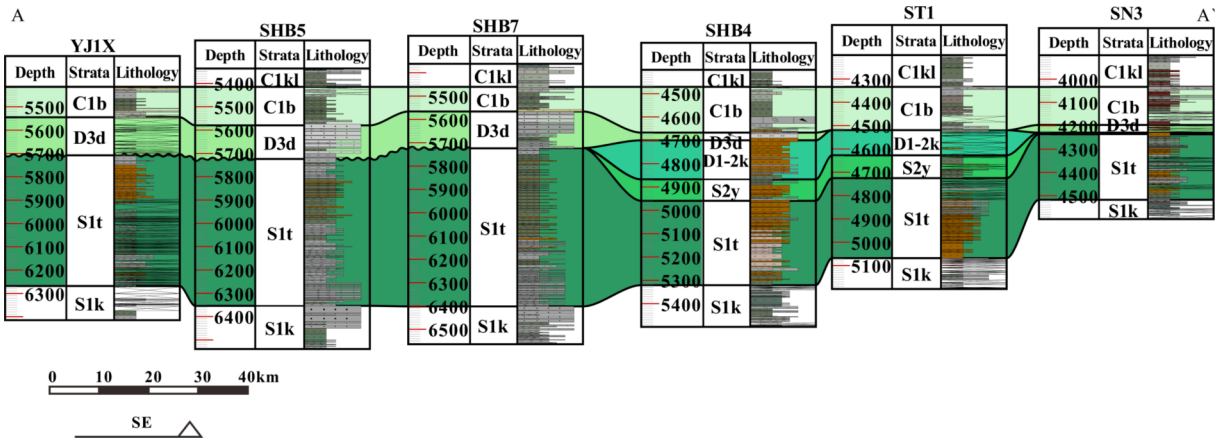

Fig. 5. Silurian well-tie profile in the Shunbei area, Tarim Basin (Wells YJ1X, SHB5, SHB7, SHB4, ST1, and SN3; location is shown in Fig. 1b).

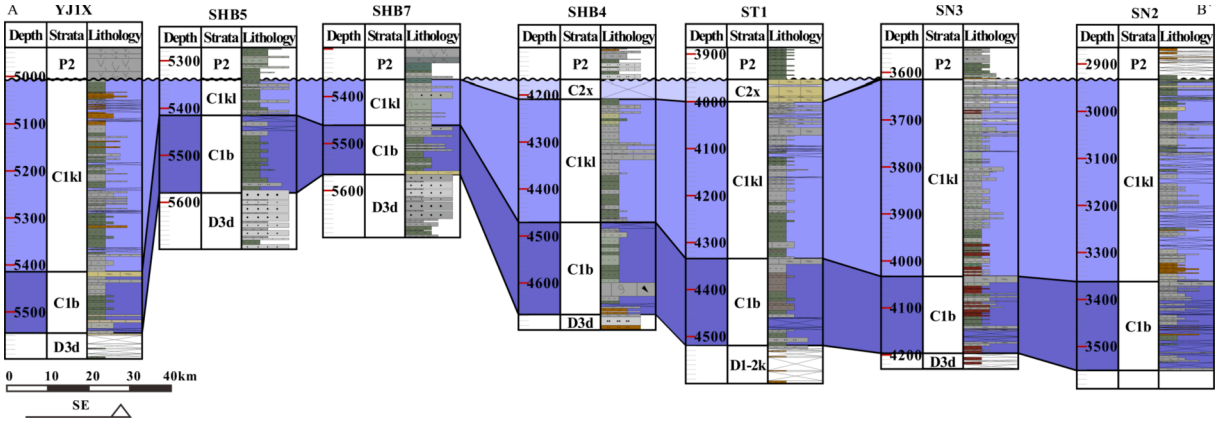

Fig. 6. Carboniferous well-tie profile in the Shunbei area, Tarim Basin (Wells YJ1X, SHB5, SHB7, SHB4, ST1, SN3, and SN2; location is shown in Fig. 1b).

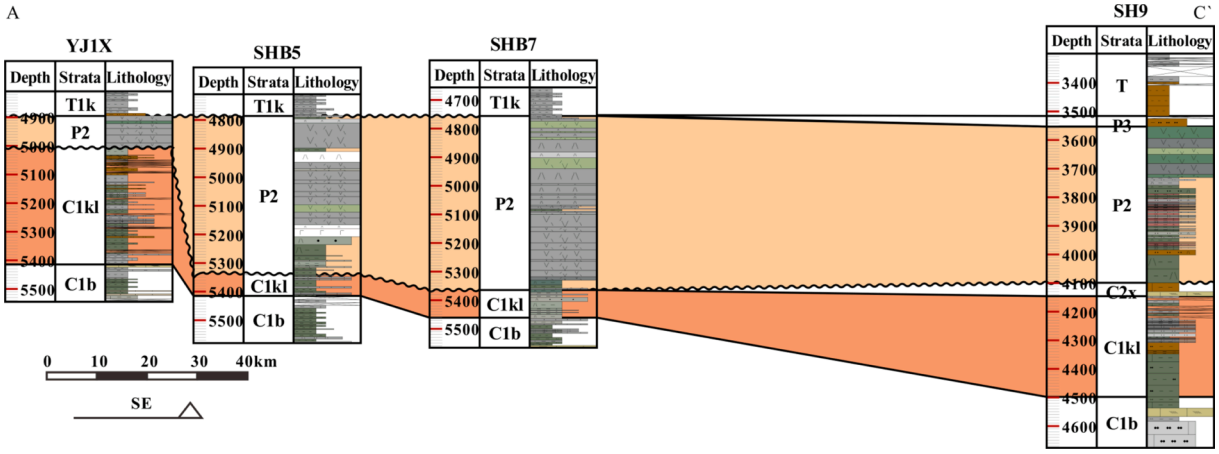

Fig. 7. Permian well-tie profile in the Shunbei area, Tarim Basin (Wells YJ1X, SHB5, SHB7, and SH9; location is shown in Fig. 1b).

intracratonic phase (Qiu et al., 2012). During the Late Ordovician to Carboniferous, the heat flow decreased gradually from ~38–43 mW/m^2 to ~36–42 mW/m^2. In the Early Permian, the heat flow increased to reach a peak of ~45–47 mW/m^2 in the Shunbei area due to the effect of the PLIPs (Li et al., 2010a). The Tarim Basin has developed into a foreland basin, and the lithosphere has thickened since the Mesozoic, resulting in the basin cooling sequentially (Zhang et al., 2007; Qiu et al., 2010; Cao et al., 2019) with the heat flow in the Shunbei area decreased slowly from ~36–40 mW/m^2 to ~33–37 mW/m^2. Noted that the heat flow in the eastern Shunbei area (e.g., Wells SHB1 and SHB2) was always higher than the western Shunbei area (e.g., Wells SHB5, SHBP1, and ZT1) in the Paleozoic and Mesozoic (Fig. 12f and Table 4).

4. Temperature fields of the middle-lower Ordovician reservoirs

The primary carbonate reservoirs are the middle-lower Ordovician Yijianfang and Yingshan Formations in the Shunbei area. Their temperature histories play an essential role in analyzing the hydrocarbon

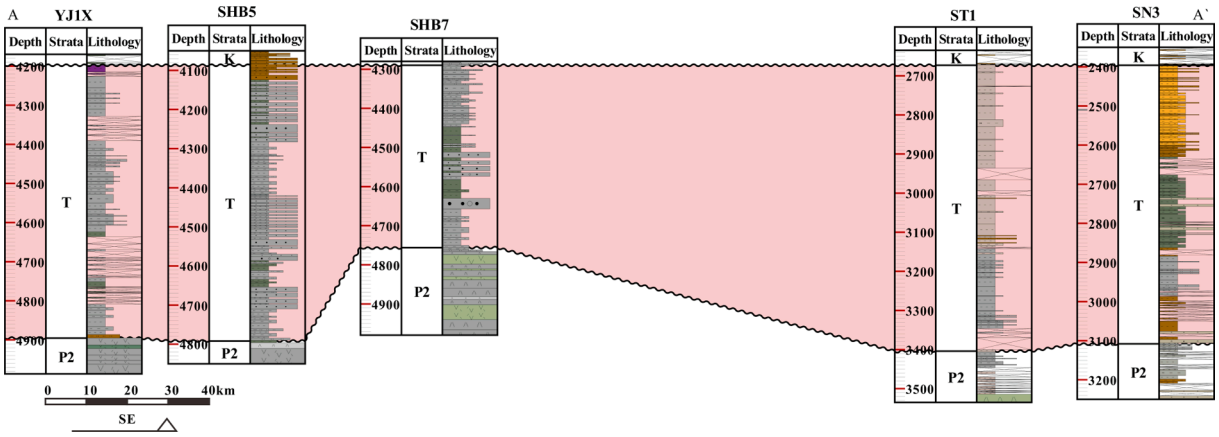

Fig. 8. Triassic well-tie profile in the Shunbei area, Tarim Basin (Wells YJ1X, SHB5, SHB7, ST1, and SN3; location is shown in Fig. 1b).

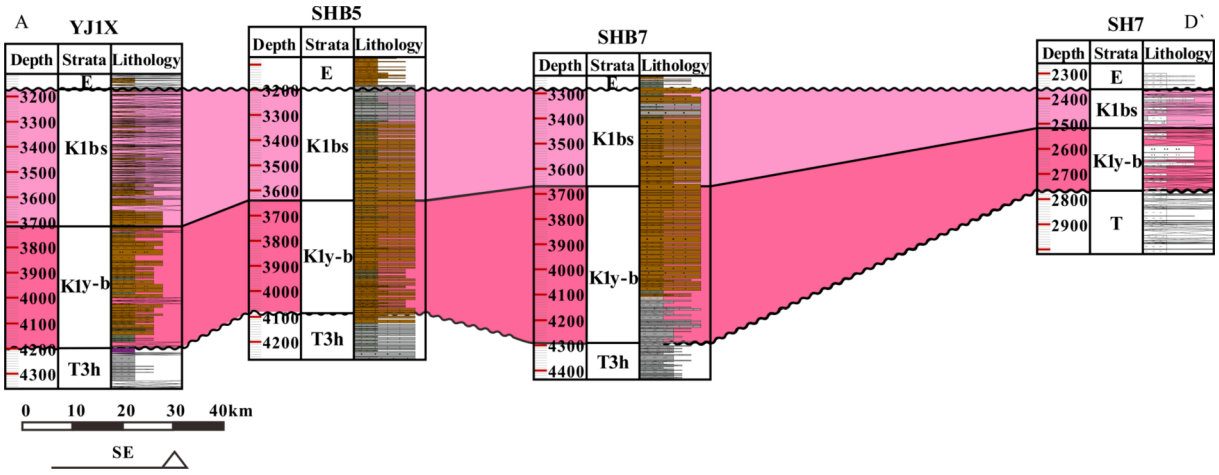

Fig. 9. Cretaceous well-tie profile in the Shunbei area, Tarim Basin (Wells YJ1X, SHB5, SHB7, and SH7; location is shown in Fig. 1b).

Table 2
Calculated erosional amounts in the Shunbei area.

Geological periods	Erosion time (Ma)	Erosion thickness (m)
Late Ordovician	445–440	150
Late Silurian	425–370	200
Late Carboniferous	300–290	210
Late Permian	258–250	40
Late Triassic	210–137	350
Late Cretaceous	80–65	190

accumulation time and oil and gas phase transformation (Fig. 13; Ren et al., 2020; Chen et al., 2020). The temperature histories of these two reservoirs show relatively complicated evolutionary trends. In this study, they were divided into three stages for presentation in brief (Fig. 13), which make no geological sense. First, the temperatures of the Yijianfang and Yingshan Formations increased rapidly from the deposition time to the Early Silurian with heating rates of 1.27 °C/Ma and 1.36 °C/Ma, respectively. As shown in Fig. 12f, the paleo-heat flow during this stage was relatively stable, so the formation temperature increment was mainly related to the rapid deposition. Secondly, the temperature of the Yijianfang and Yingshan Formations increased slowly with the heating rates < 0.1°C/Ma from Middle Silurian to the end of the Paleogene. The long-term low temperature and low heating rate are suitable for preserving liquid hydrocarbons. Finally, the rapid subsidence since the Neogene led to the rapid temperature increase of the Yijianfang and Yingshan Formations again in the Shunbei area with the heating rates of 1.20 °C/Ma and 1.28 °C/Ma, respectively. The highest temperatures experienced by the Yijianfang and Yingshan Formations are 150 °C and 163 °C, respectively.

5. Hydrocarbon accumulation period in the Shunbei area

Fluid inclusions are small volumes of paleo-fluids sealed in minerals that are not affected by foreign substances, which provide essential information about geological processes (Randive et al., 2014). Analyzing the paleotemperature information recorded by the fluid inclusions usually involves testing the temperature parameters such as homogenization temperature (T_h), decrepitation temperature (T_d), freezing temperature (T_f), melt temperature (T_m), and trapping temperature (T_t) (Lu et al., 2004, 2017). The T_h of fluid inclusions is considered a valuable parameter for recognizing hydrocarbon charging histories (Karlsen et al., 1993; Wang et al., 2002). Fluid inclusions may be rebalanced in the sedimentary diagenetic environment, causing the measured temperature data of fluid inclusions to not accurately express the initially captured information (Lu et al., 2020). Therefore, the fluid inclusion assemblage (FIA), which can show the simultaneity of fluid inclusions capture, is usually used to examine the reliability of fluid inclusions (Goldstein and Reynolds, 1994). The FIA represents a group of fluid inclusions with variable sizes and shapes captured simultaneously, and their T_h is consistent (variation less than 10 °C) (Goldstein and Reynolds, 1994; Chi and Lu, 2008). This study collected the calcite samples of Ordovician Yijianfang and Yingshan Formation reservoirs from the Well SHB2 for petrography and T_h analysis of FIAs (Fig. 14 and Table 5). The

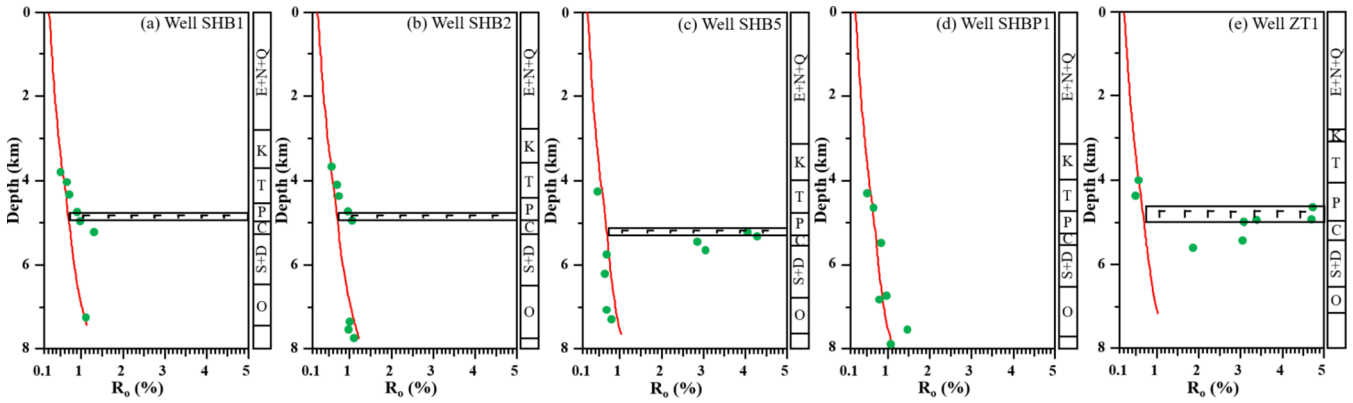

Fig. 10. Equivalent vitrinite reflectance (R_{equ}) data versus depth for the Shunbei area. Green dots indicate measured R_{equ} data, the solid red line indicates modeled result, and the lithologic column indicates intrusive basaltic rock. Є=Cambrian; O = Ordovician; D = Devonian; S = Silurian; C = Carboniferous; P = Permian; T = Triassic; K = Cretaceous; E = Paleogene; N = Neogene and Q = Quaternary. (For interpretation of the references to colour in this figure legend, the reader is referred to the web version of this article.)

Table 3
Equivalent vitrinite reflectance data of the typical wells in the Shunbei area.

Well No.	Depth (m)	Formation	R_{equ} (%) [+]	Well No.	Depth (m)	Formation	R_{equ} (%) [+]
SHB5	4,280	T	0.45		6,764	S	0.98*
	5,242	P	4.05		6,836	S	0.80*
	5,320	P	4.29		7,550	O	1.48*
	5,460	C	2.87*		7,975	O	1.06*
	5,680	D	3.06*	SHB2	3,712	T	0.54
	5,770	S	0.70*		4,100	T	0.67
	6,232	S	0.66*		4,381	T	0.74
	7,080	O	0.68*		4,721	P	0.96
	7,312	O	0.80*		4,958	P	1.03
ZT1	3,986	T	0.57		7,362	O	1.00*
	4,360	P	0.50		7,526	O	0.94*
	4,656	P	4.85		7,738	O	1.11*
	4,934	P	4.79	SHB1	3,800	T	0.51
	4,950	C	3.47*		4,050	T	0.65
	5,008	C	3.15*		4,350	T	0.72
	5,404	C	3.11*		4,750	P	0.90
	5,578	D	1.92*		4,950	C	1.00*
SHBP1	4,320	T	0.50		5,250	C	1.30*
	4,725	T	0.64		7,250	O	1.10*
	5,502	C	0.84*				

[+] Some vitrinite reflectance (R_o) data in the upper Paleozoic and the Mesozoic strata are equal to the equivalent vitrinite reflectance (R_{equ}) in our study for consistency. The R_{equ} values with asterisks (*) were calculated from bitumen reflectance (R_b) using the following formulae: $R_{equ} = 0.618R_b + 0.40$ ($R_b < 2.0\%$; Jacob, 1989); $R_{equ} = 0.688\ R_b + 0.346$ ($R_b > 2.0\%$; Liu and Shi, 1994). O = Ordovician; D = Devonian; S = Silurian; C = Carboniferous; P = Permian; T = Triassic.

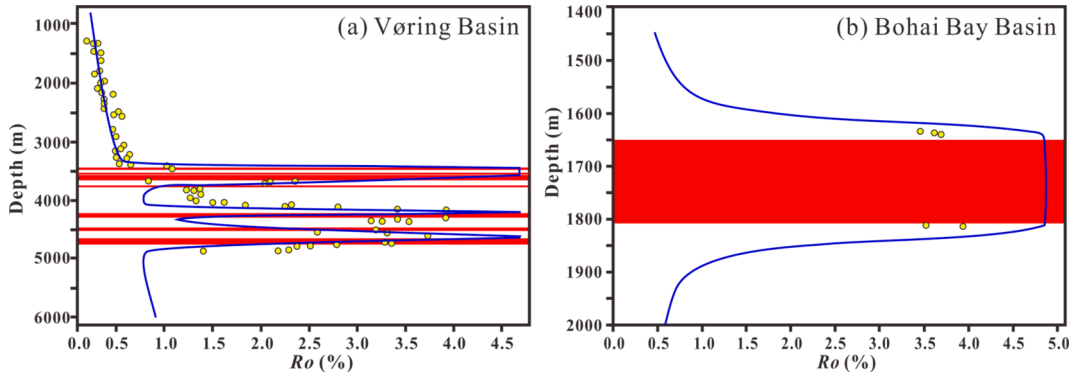

Fig. 11. Vitrinite reflectance (R_o) data versus depth for the Vøring Basin in Norway (Fjeldskaar et al., 2008) and Bohai Bay Basin in China (Wang et al., 2011). The yellow circle indicates measured R_o data, the solid blue line indicates modeled result, and the red rectangle indicates magmatic intrusions. (For interpretation of the references to colour in this figure legend, the reader is referred to the web version of this article.)

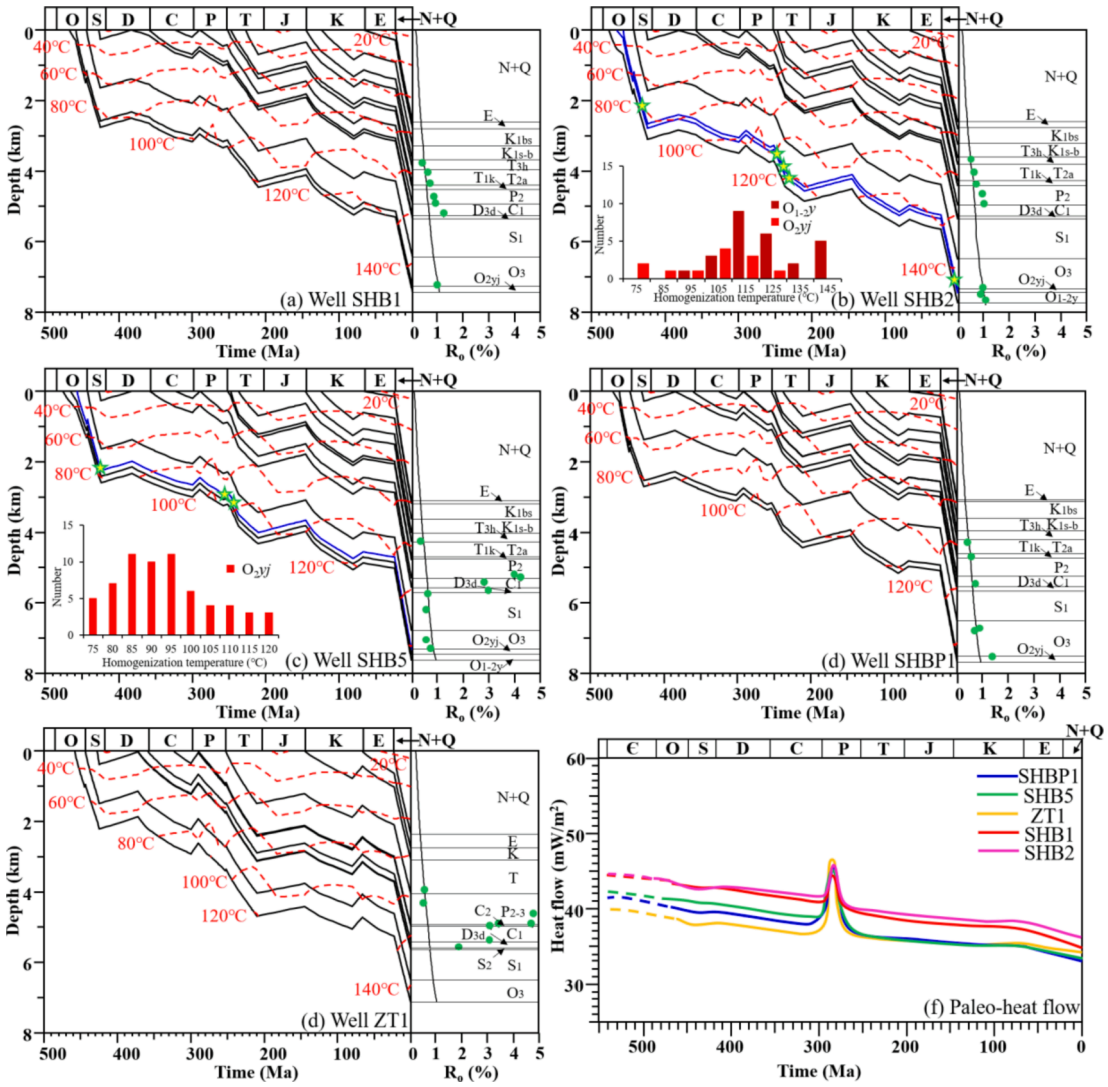

Fig. 12. The buried, thermal, and heat flow evolution histories of the typical wells in the Shunbei area. The solid lines indicate the modeled results, and the green dots indicate the measured vitrinite reflectance in the right panel in (a)–(e). Inserted histograms show the homogenization temperature distribution of the coeval aqueous fluid inclusions in FIAs. The blue lines represent the reservoirs, and the green stars show the timing of hydrocarbon filling and entrapment. (For interpretation of the references to colour in this figure legend, the reader is referred to the web version of this article.)

Table 4
A summary of the paleo-heat flow modeling results in this study (mW/m^2).

Well No.	Structural location	Cambrian	Ordovician	Silurian–Carboniferous	Early Permian	Mesozoic	present
SHB1	Shunbei No. 1 strike-slip fault zone	45–44	44–43	43–41	45	39–37	35
SHB2	Shunbei No. 1 secondary fault zone	45–44	44–43	43–42	46	40–38	37
SHB5	Shunbei No. 5 strike-slip fault zone	43–42	42–41	41–39	45	37–35	34
SHBP1	Secondary strike-slip fault zone between the Shunbei No. 5 and No. 7 strike-slip fault zones	42–41	41–39	39–38	46	37–35	33
ZT1	Western slope of the Katake Uplift	40–49	39–38	38–36	47	36–35	34

fluid inclusions microthermomertry was performed at the State Key Laboratory of Petroleum Resources and Prospecting, China University of Petroleum-Beijing, using the LinKam THMS G600 heating-freezing stage and Leica DMR microscope. Finally, we analyzed the charging time of the Ordovician reservoirs in the SHB2, SHB1-3, SHB1-7, SHB5, and SHB7 well block according to the reconstructed burial and thermal histories and T_h data in this paper and previous studies (Wang, 2019; Wang et al., 2019, 2020).

As shown in Fig. 14, the Ordovician Yingshan Formation fluid inclusions in the Shunbei area were found in the carbonate rock with the cracks and pores filled by sparry calcite cement. Meanwhile, calcite cement can be divided into two generations. The yellowish-brown calcite cement belonged to the first generation and developed along the crack wall with the vertical direction, then filled by the second generation of calcite cement (Fig. 14a). Interestingly, the second generation of calcite cement is probably destroyed by the tectonic movements and filled with bitumen (Fig. 14a and 14b). The Ordovician Yijianfang and Yingshan Formation reservoirs in the SHB2 well block developed secondary inclusions through petrographic evidence, including liquid-only oil inclusions, liquid-only aqueous inclusions, and

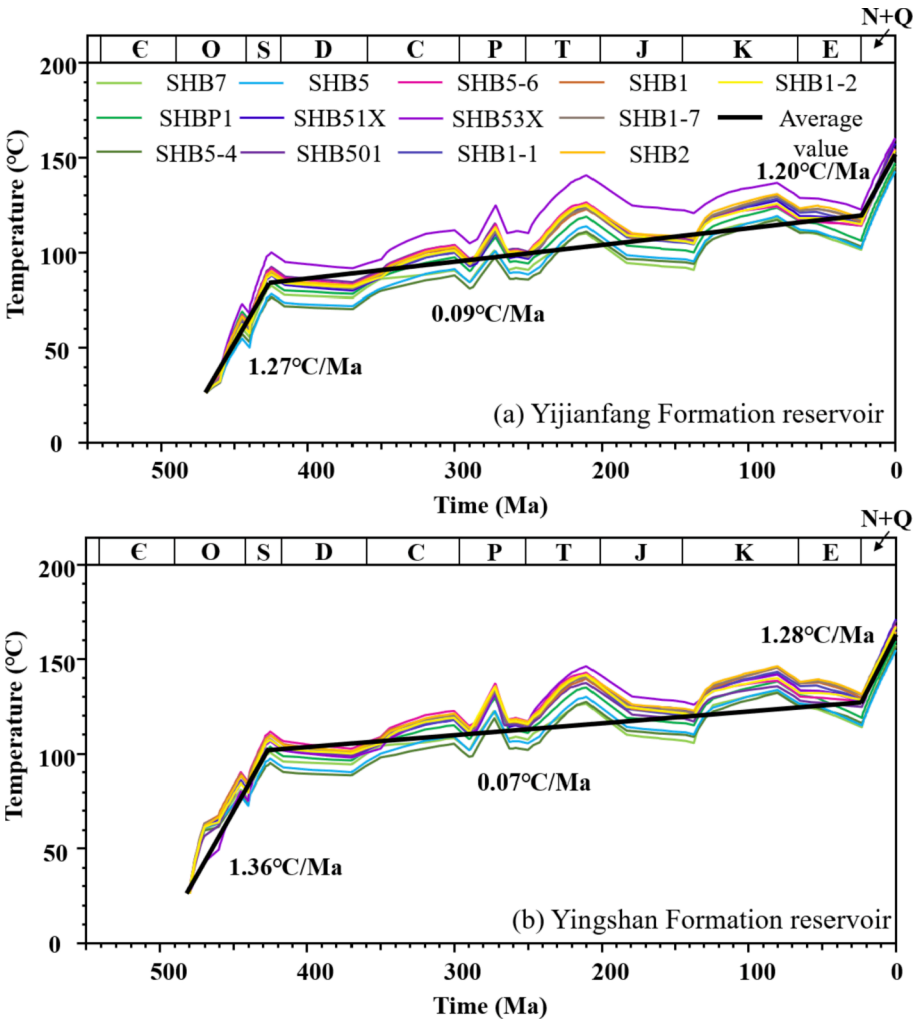

Fig. 13. Temperature evolution histories of middle-lower Ordovician formations in typical wells in the Shunbei area: (a) Yijianfang Formation reservoir and (b) Yingshan Formation reservoir.

liquid-dominated biphase aqueous inclusions (Fig. 14). The Yingshan Formation developed two phases of coeval aqueous inclusions in six FIAs with the peak T_h of 114.1–124.3 °C and 140.3–149.6 °C, while the Yijianfang Formation developed two phases of coeval aqueous inclusions in three FIAs with the peak T_h of 76.3–88.2 °C and 100.3–107.5 °C (Table 5). According to the burial and thermal histories, we considered that the hydrocarbon charging in the SHB2 well block occurred in 435–430 Ma, 250–235 Ma, and 5–3 Ma, which are isochronous with the intensive tectonic movements in the Tarim Basin and adjacent areas (Fig. 12b; He et al., 2005). The T_h data indicates the hydrocarbon charging periods among the strike-slip fault zones in the Shunbei area are different. The No. 1 strike-slip fault zone (Wells SHB2, SHB1-3, and SHB1-7) experienced three periods of hydrocarbon charging occurred in 435–420 Ma, 263–220 Ma, and 18–3 Ma, respectively (Fig. 12b, 15a, and 15b), whereas the No. 5 (Well SHB5) and No.7 (Well SHB7) strike-slip fault zones just experienced the two periods that occurred in 435–420 Ma and 263–220 Ma, respectively (Fig. 12c and 15c). These results are consistent with the previous studies using microphotoluminescence spectra (Han et al., 2021), homogenization temperature data (Wang et al., 2020; Han et al., 2021), and PVT simulation of fluid inclusion (Chen et al., 2020), as well as the present-day oil and gas geochemical characteristics (Qi, 2020).

6. Discussion

6.1. Temporal-spatial thermal history in the Tarim Basin

Due to the differential tectonic setting, basement relief, and lithology, the heat flow histories of the secondary tectonic units in the Tarim Basin are different (Fig. 16). The uplift region with a high basement usually shows a higher geothermal gradient and heat flow than the depression region with a relatively low basement. This is because the depression region of the sedimentary basin deposits significantly more sandstone and mudstone sediments with lower thermal conductivity, while the uplift region preserves relatively thick bedrock with higher thermal conductivity. This difference in the rock thermal conductivity leads to the "thermal refraction" effect between uplift and depression regions, which in turn leads to the accumulation of heat energy in the uplift regions (Xiong and Gao, 1982; Chang et al., 2017). Finally, the depression region of the sedimentary basins develops into a relatively low-temperature zone compared to the uplift region. The Shaya, Katake, Bachu, and Guchengxu areas developed as paleo-uplifts since the Early Paleozoic, and therefore their paleo-heat flow was always higher than that of the Shunbei area (Fig. 16). It is noted that the heat flow of the Bachu Uplift gradually increased from the Late Cambrian to the Early Silurian, which is different from other secondary tectonic units in the Tarim Basin. It was related to the higher thermal conductivity of the 800–1,000 m thick gypsum and salt units in the middle Cambrian strata

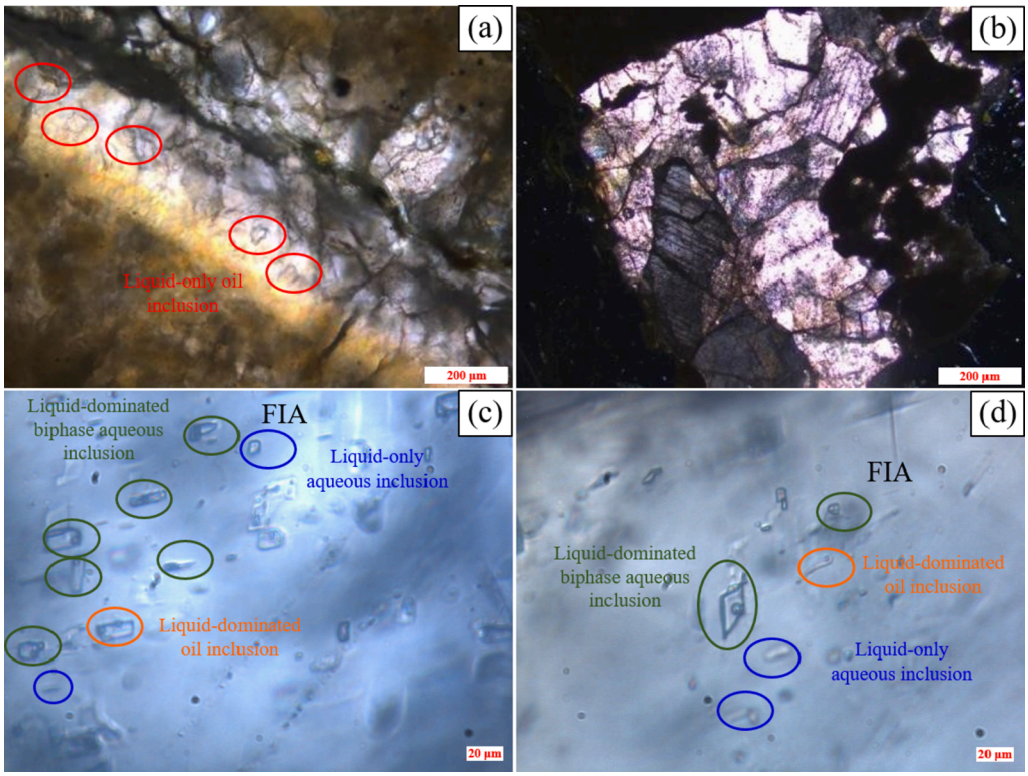

Fig. 14. Photomicrographs of fluid inclusions of calcite in Well SHB2. (a) liquid-only oil inclusions in cracks filled with asphalt and calcite (the red circles), transmitted light, $O_{1\text{-}2}y$, 7,521 m, calcirudite; (b) bitumen in calcite filling pores, transmitted light, $O_{1\text{-}2}y$, 7,738 m, micritic limestone; (c) and (d) liquid-dominated oil inclusions (the orange circles), liquid-only aqueous inclusions (the blue circles) and liquid-dominated biphase aqueous inclusion (the green circles) detected in calcite filled caves, transmitted light, $O_{1\text{-}2}y$, 7,523 m, bioclast limestone. (For interpretation of the references to colour in this figure legend, the reader is referred to the web version of this article.)

Table 5
Homogenization temperature data for fluid inclusions from typical wells in the Shunbei area, Tarim Basin.

Well No.	Depth (m)	Formation	FIA	N	Type	Host minerals	Range of T_h (°C)	Average of T_h (°C)
SHB2	7,521	$O_{1\text{-}2}y$	FIA1	3	Liquid-only aqueous inclusion	Calcite	103.7–113.4	109.8
SHB2	7,521	$O_{1\text{-}2}y$	FIA2	10	Liquid-only aqueous inclusion	Calcite	114.1–124.3	119.5
SHB2	7,521	$O_{1\text{-}2}y$	FIA3	3	Liquid-only aqueous inclusion	Calcite	125.8–127.9	126.8
SHB2	7,521	$O_{1\text{-}2}y$	FIA4	3	Liquid-dominated biphase aqueous inclusion	Calcite	128.4–132	129.9
SHB2	7,521	$O_{1\text{-}2}y$	FIA5	5	Liquid-dominated biphase aqueous inclusion	Calcite	140.3–149.6	145.8
SHB2	7,521	$O_{1\text{-}2}y$	FIA6	2	Liquid-dominated biphase aqueous inclusion	Calcite	151.0–151.5	151.3
SHB2	7,360	O_2yj	FIA7	3	Liquid-only aqueous inclusion	Calcite	76.3–88.2	81.1
SHB2	7,360	O_2yj	FIA8	3	Liquid-only aqueous inclusion	Calcite	100.3–107.5	104.5
SHB2	7,361	O_2yj	FIA9	6	Liquid-only aqueous inclusion	Calcite	113.4–126.9	119.0
SHB5	7,425–7,427	O_2yj			Liquid-only aqueous inclusion	Calcite	73.5–127.0*	
SHB7	7,729–7,733	$O_{1\text{-}2}y$			Liquid-only aqueous inclusion	Calcite	73.7–109.6*	
SHB1-3	7,266–7,289	O_2yj			Liquid-only aqueous inclusion	Calcite	69.3–133.7*	
SHB1-7	7,350–7,357	O_2yj			Liquid-only aqueous inclusion	Calcite	86.6–152.8*	

T_h is the homogenization temperature (°C); * indicates that the test data is obtained from previous studies (Wang, 2019, Wang et al., 2019, 2020).

(Qiu et al., 2012). In addition, the thermal effect of the PLIPs during the Early Permian was just recorded by the heat flow histories of the Shunbei area and Shaya Uplift (Fig. 16).

6.2. *Hydrocarbon charging of the lower Paleozoic strata in the Tarim Basin*

According to the homogenization temperature and fluorescent spectrum of fluid inclusions, crude oil *Re-Os* ages and sandstone *K-Ar* ages (Chen et al., 2010, 2014; Xing et al., 2011; Zhao et al., 2011; Shi et al., 2012; Zhang, 2016; Li, 2017), the hydrocarbon charging of the lower Paleozoic carbonate reservoirs in the Tarim Basin could be divided into three stages: Late Ordovician–Late Silurian (463–420 Ma), Permian–Triassic (298–200 Ma) and Paleogene–Quaternary (65–3 Ma) (Fig. 17), which matches the important period of tectonic transformation in the Tarim Basin (Zhu et al., 2010; Zhang et al., 2011). However, the hydrocarbon charging process among the secondary structural units in the Tarim Basin was different.

Previous studies considered that the hydrocarbon charging process in the Shunbei area was related to the formation and activity of the strike-slip fault zones (Wang et al., 2020; Han et al., 2021). Due to the southward subduction of the Tianshan Ocean in the Late Ordovician, the No. 1 strike-slip fault zone was reactivated and became a channel for oil migration (Deng et al., 2018), which contributed to the first hydrocarbon charging in the Shunbei area. During the Permian, the Tarim Basin entered a crucial period of hydrocarbon generation and expulsion along with the reactivation of the strike-slip fault zones, providing the opportunity for the second hydrocarbon migration and charging (Deng et al., 2018; Han et al., 2021). During the Neogene, the No. 1 strike-slip fault zone was in a tectonic setting of transtension with the distant effect of the collision between the India and Eurasia plates (Zhang et al., 2007), which provides another good opportunity for the third hydrocarbon charging from the deep lower Cambrian source rocks to the shallow Ordovician reservoirs (Liu, 2020). Han et al. (2021) considered that the lower Cambrian source rock in the Manjiaer Depression was the hydrocarbon center for the Shaya Uplift, Katake Uplift, and Shuntuogole

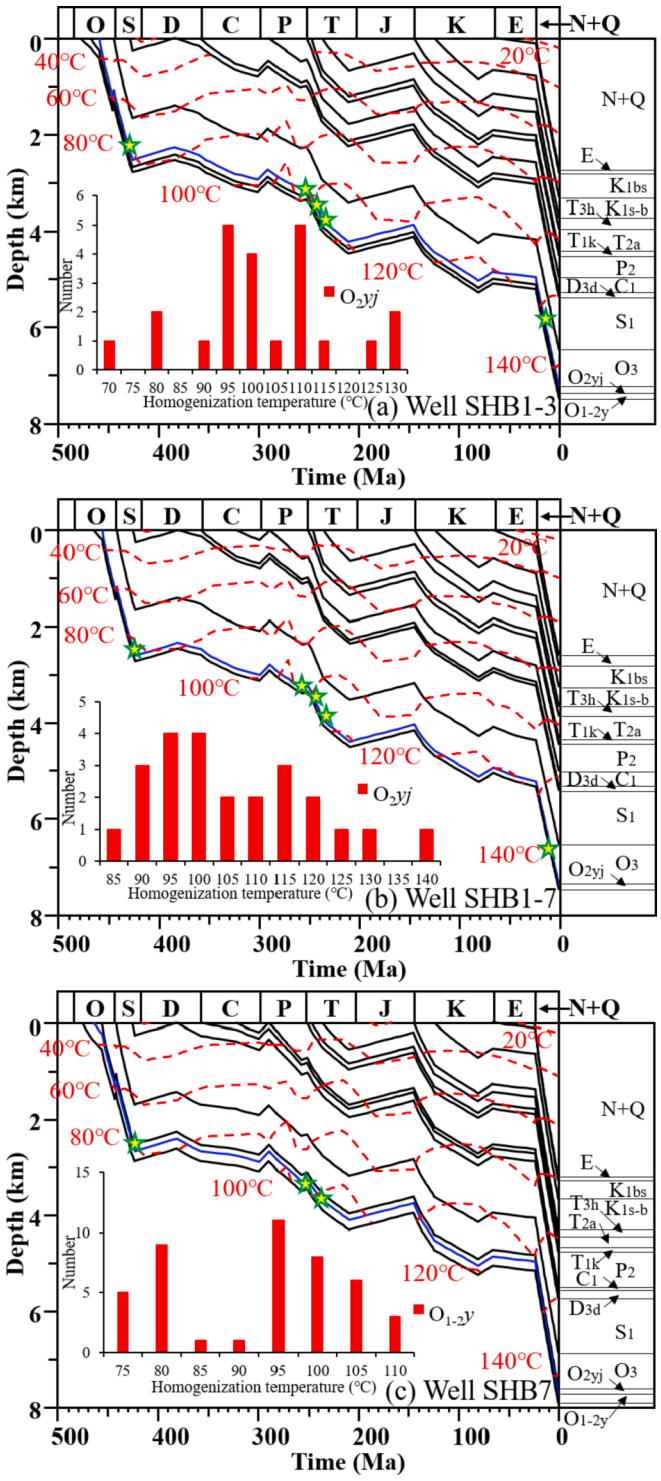

Fig. 15. Burial and temperature histories of the wells in the Shunbei area. Inserted histograms show the homogenization temperature distribution of the coeval aqueous fluid inclusions. The blue lines represent the reservoir, and the green stars show the timing of hydrocarbon filling and entrapment. (a) Well SHB1-3, O_2yj, 7,256–7,358 m; (b) Well SHB1-7, O_2yj, 7,339–7,456 m and (c) Well SHB7, $O_{1\text{-}2}y$, 7,728–7,733 m. (For interpretation of the references to colour in this figure legend, the reader is referred to the web version of this article.)

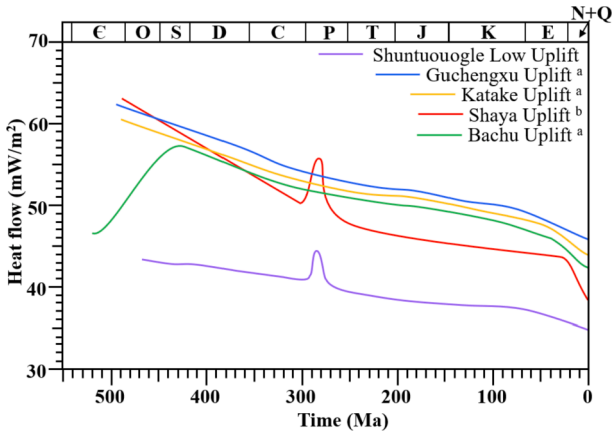

Fig. 16. Heat flow evolution histories of different tectonic units in Tarim Basin. [a] Qiu et al., 2012; Liu et al., 2021; [b] Li et al., 2010a.

Low Uplift. Compared to the No. 5 and 7 strike-slip fault zones in the Shunbei area, the No. 1 strike-slip fault zone is closer to the Manjiaer Depression and experienced the last oil charging process (Fig. 17). The third stage of hydrocarbon charging in the Shunbei area is dominated by oil and gradually transitions to gas in the Shunnan area, which is due to the more solid bitumen bearing hydrocarbon inclusions, dry gas inclusions, and intense thermochemical sulfate reduction (TSR) in the Shunnan area (Chen et al., 2020).

The Cambrian reservoirs in the Katake Uplift lack the Permian–Triassic hydrocarbon charging period (Liang, 2019; Shi et al., 2012; Chen et al., 2014; Fig. 17). Liang (2019) considered that the formation of large faults during the Early Devonian provided the opportunity that the crude oil from the lower Cambrian source rocks just went through (did not stay in) the Cambrian reservoirs and then got directly into the upper Ordovician and Silurian reservoirs, which were recorded by biomarker compound and fluid inclusions (Hu et al., 2015; Wang et al., 2015; Zhu et al., 2007). The Ordovician reservoirs in the Katake Uplift lack the Late Ordovician–Late Silurian hydrocarbon charging period, which may be related to its structural location that is not conducive to oil and gas charging (Fig. 17; Wu et al., 2020; Xing et al., 2011).

The middle-lower Ordovician reservoirs around the Tahe Oilfield in the Shaya Uplift lack the Permian–Triassic hydrocarbon charging period, and that in the Yuqi area only has the Paleogene–Quaternary hydrocarbon charging (Fig. 17). The differential structural evolution was probably responsible for the lack of hydrocarbon charging during the Permian–Triassic around the Tahe oilfield (Zhang et al., 2011; Chen et al., 2014).

Interestingly, the lower Cambrian source rocks in the Maigaiti Slope were immature during the Late Ordovician-Late Silurian and cannot generate oil, so the Yingshan Formation reservoirs lack the Late Ordovician–Late Silurian hydrocarbon charging period (Fig. 18; Si et al., 2013; Wu et al., 2017). Due to the differential tectonic uplift, burial, and thermal histories, the middle-lower Ordovician reservoirs of Wells SN4, SN1, TZ45, and XK7 and the Cambrian reservoirs of Well ZS5 accumulated natural gas since the Paleogene. In contrast, the crude oil charged the lower Paleozoic reservoirs of other wells (Fig. 17).

6.3. *Thermal history of the lower Cambrian source rocks in the Shunbei area*

Although some oil and gas reservoirs have been found in the Ordovician Formation of the Shuntuoguole Low Uplift, Shaya Uplift, and Katake Uplift in the central Tarim Basin, it is still controversial for their origin from the lower Cambrian Yuertusi Formation or the middle-upper Ordovician source rocks (Zhang et al., 2000, 2002, 2008; Zhang and Huang, 2005; Li et al., 2010b, 2011, 2012b, 2015; Yu et al., 2011; Yang

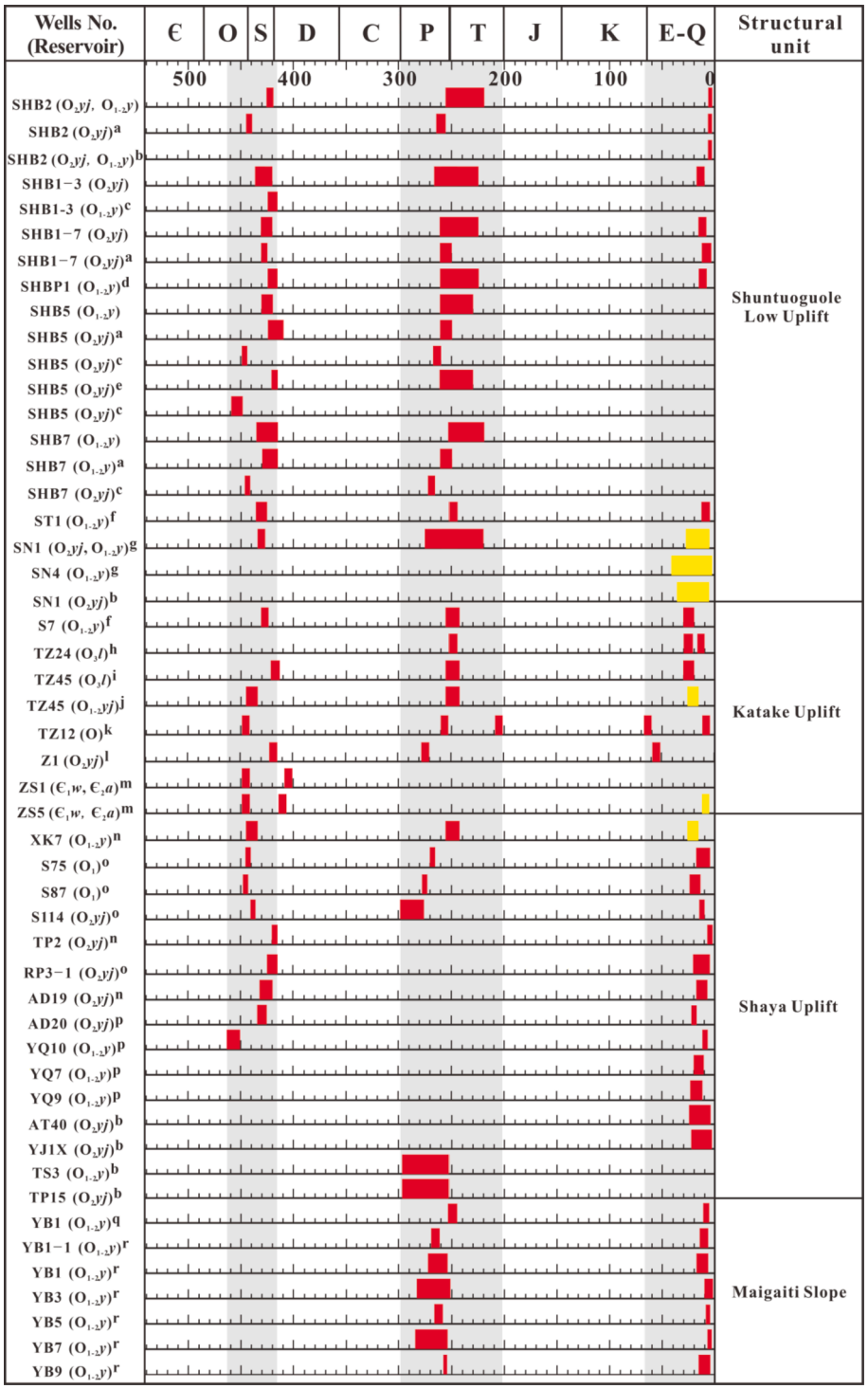

Fig. 17. Schematic diagram of the chronology of hydrocarbon charging in the Cambrian-Ordovician marine carbonate reservoirs in the Tarim Basin. The red square represents oil charging, and the yellow square represents gas charging. (Location is shown in Fig. 1b and c). [a] Han et al., 2021; [b] Chen et al., 2020; [c] Lu et al., 2020; [d] Kang, 2019; [e] Wang et al., 2020; [f] Zhang, 2016; [g] Wang, 2019; [h] Xing et al., 2011; [i] Zhao et al., 2011; [j] Li, 2017; [k] Chen et al., 2010; [l] Zhang, 2021; [m] Liang, 2019; [n] Shi et al., 2012; [o] Ni et al., 2016; p Chen et al., 2014; [q] Si et al., 2013; [r] Wu et al., 2017. (For interpretation of the references to colour in this figure legend, the reader is referred to the web version of this article.)

et al., 2016; Gu et al., 2019, 2020a, 2020b; Qi, 2020). According to the C_{23} tricyclic terpene content and distribution characteristic of the C_{27}-C_{28}-C_{29}ααα20R regular steranes, Gu et al. (2020a) considered that the crude oil from middle-lower Ordovician reservoirs in the Shunbei area has a good affinity with the lower Cambrian source rocks in the Kalpin Uplift and Kongquehe Slope. Therefore, this study evaluated the maturation evolution history of the lower Cambrian source rocks in the Shunbei area, providing some new insights for oil and gas generation time (Fig. 18). Because the bottom of all the wells in the Shunbei area did not reach the lower Cambrian source rocks, we cannot but calculate the formation thickness below the bottom of the wells by using the seismic data. Meanwhile, the Cambrian heat flow was inferred based on the evolutionary trend of the heat flow histories (Fig. 12f). Finally, the maturation evolution histories of the lower Cambrian source rocks in the Shunbei area were obtained based on the reconstructed burial and heat flow histories since the Cambrian (Fig. 18).

The lower Cambrian source rocks began to generate oil during the Early Ordovician when its maturity was more than 0.5%. The maturity of the lower Cambrian source rocks reached 0.9%–1.4% during the Early–Middle Silurian, which can provide oil and gas for the middle-lower Ordovician reservoirs, as revealed by fluid inclusion. During the Middle Silurian–Late Carboniferous, the maturity of the lower Cambrian

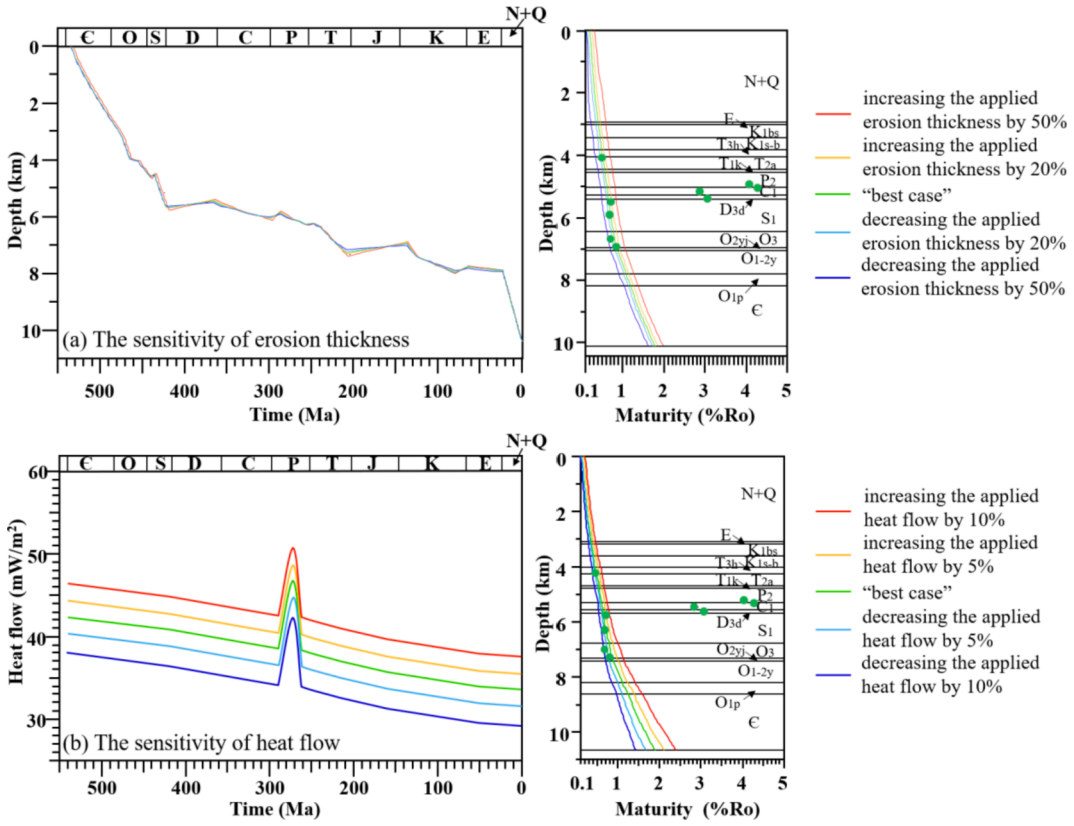

Fig. 18. Maturation histories of lower Cambrian Yuertusi Formation source rocks of the studied wells in the Shunbei area. The dotted line represents the maturity histories of the predicted bottom depth of the source rocks.

source rocks exceeded 1.3% and should begin to generate wet gas. However, the high-pressure environment (The average value and coefficient of pressure are 88 MPa and 1.1, respectively) since the Middle Silurian in the Shunbei area probably inhibited the thermal history of the source rocks and increased the upper limit of the liquid oil generation window by ~0.5% (Hao et al., 1995; McTavish, 1998; Wu et al., 2016; Gu et al., 2019; Ren et al., 2020). It should be a piece of evidence that the middle-lower Ordovician reservoirs keep the crude oil at the present-day. The temperature and maturity of the Yuertusi Formation source rocks in the Shunbei area gradually increased from northwest to southeast (Figs. 18 and 19), which was controlled by the burial depth (9,400–10,400 m; Wu et al., 2022) and paleo-heat flow (this study).

It should point out that the temperature and maturity of the Yuertusi Formation source rocks in the Shunbei area are affected by the burial and thermal modeling results. For assessing the accuracies of the burial and thermal histories, we test the error of the reconstructed erosion

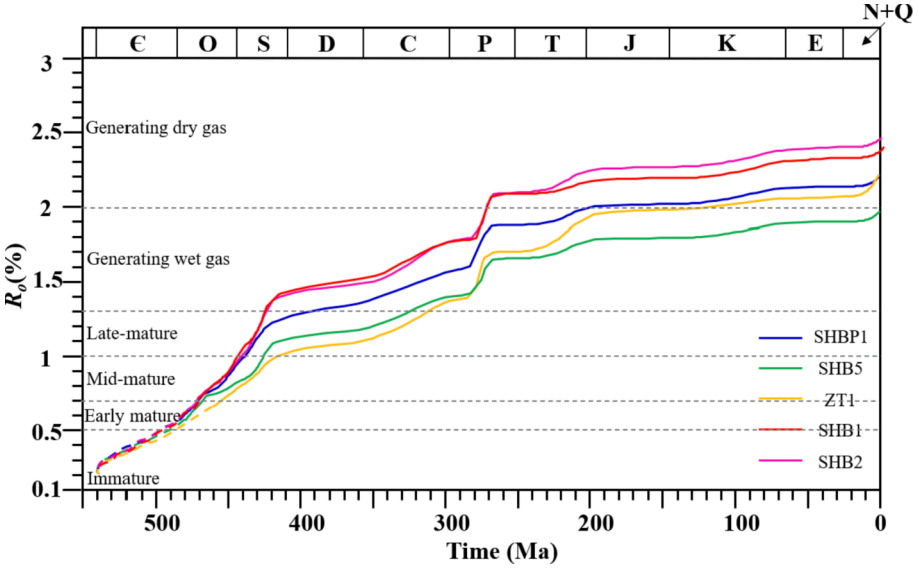

Fig. 19. Spatial distribution of the temperature and maturity evolution of the Yuertusi Formation source rocks in the Shunbei area with the oil–gas geochemical characteristics.

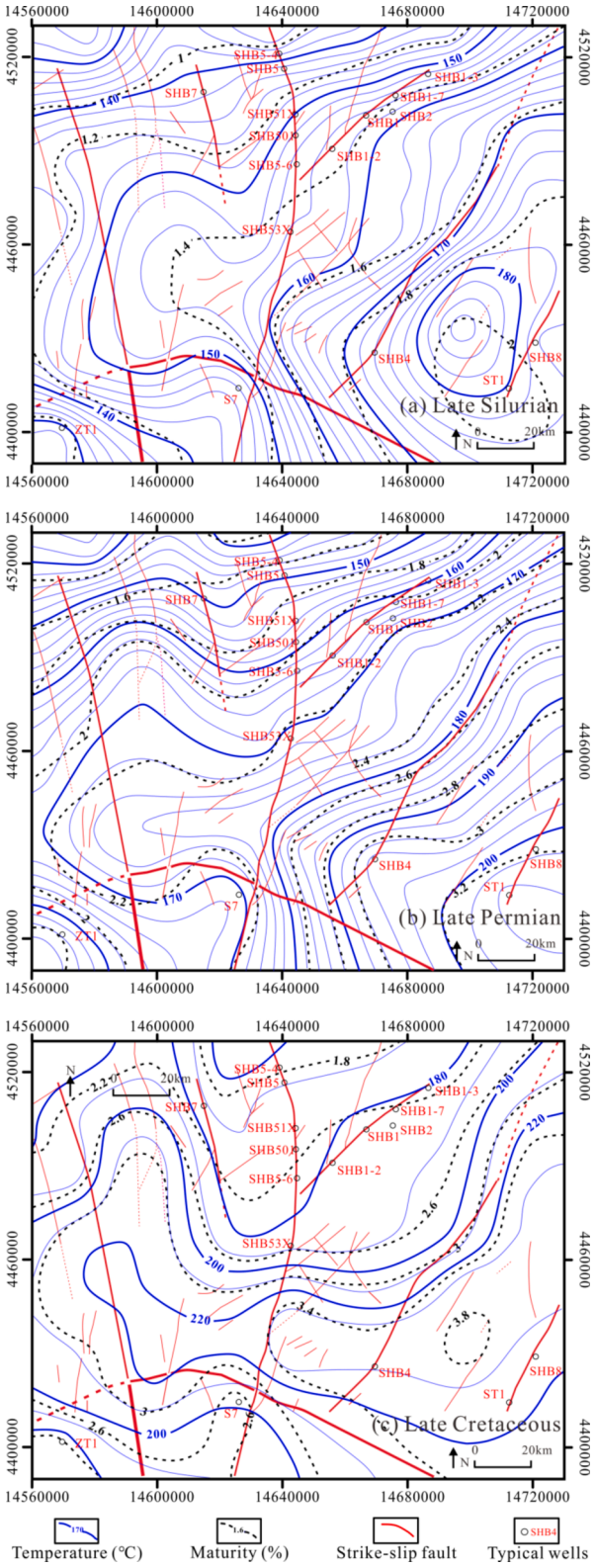

Fig. 20. Sensitivity of the erosion thickness (a) and the heat flow (b) on the modeled % R_o profiles (calculated from the "best case" model) for Well SHB5. The sensitivity test of the erosion thickness is performed by increasing or decreasing the applied erosion thickness by 20% and 50%. Perform the heat flow sensitivity test by increasing or decreasing the applied heat flow by 5% and 10%. The green dots indicate the measured vitrinite reflectance data in the right panel. (For interpretation of the references to colour in this figure legend, the reader is referred to the web version of this article.)

thickness and heat flow values (Fig. 20). The measured R_{equ} and modeled R_o show a good uniformity when the erosion thickness and heat flow vary with the error of ± 20% and ± 5%, respectively.

7. Conclusions

This study documented the paleo-heat flow for the Shunbei area in the Tarim Basin based on the calculated erosion thickness and measured equivalent vitrinite reflectance data, which decreased gradually from ~38–43 mW/m^2 in the Late Ordovician to ~33–37 mW/m^2 at the present-day. Noted that there is an abrupt peak of ~45–47 mW/m^2 during the Early Permian, which resulted from the intensive magmatic activity. Due to the paleo-heat flow and burial depth, the Yijianfang and Yingshan Formation reservoirs experienced an evolutionary process of rapid heating–slow heating–rapid heating after the deposition. We recognized that the hydrocarbon charging periods among the strike-slip fault zones in the Shunbei area were differential according to the homogenization temperature data of fluid inclusion assemblage.

CRediT authorship contribution statement

Dan Li: Conceptualization, Data curation, Formal analysis, Methodology. **Jian Chang:** Supervision, Project administration, Funding acquisition. **Nansheng Qiu:** . **Jiangshan Wang:** Data curation. **Mengran Zhang:** Data curation, Visualization. **Xian Wu:** Resources. **Jun Han:** Project administration, Resources. **Huili Li:** Resources. **Anlai Ma:** Resources.

Declaration of Competing Interest

The authors declare that they have no known competing financial interests or personal relationships that could have appeared to influence the work reported in this paper.

Acknowledgements

This work was granted by the National Natural Science Foundation of China (No. U19B6003) and the National Key Research and Development Program of China (No. 2017YFC0603102).

References

Buchardt, B., Lewan, M.D., 1990. Reflectance of vitrinite-like macerals as a thermal maturity index for Cambrian-Ordovician alum shale, southern Scandinavia. AAPG Bull. 74, 394–406.

Cao, H.Z., He, L.J., Zhang, L.Y., 2019. Inversion of background thermal history since the formation of the Tarim Craton. Chin. J. Geophys. 62, 236–247 in Chinese with English abstract.

Chang, J., Brown, R.W., Yuan, W.M, Li, W.Z, Que, Y.Q, Qiu, N.S, 2014. Mesozoic cooling history of the "Bachu Uplift" in the Tarim Basin, China: Constraints from zircon fission-track thermochronology. Radiat. Meas. 67, 5–14.

Chang, J., Li, D., Min, K., Qiu, N.S, Xiao, Y., Wu, H., Liu, N., 2019. Cenozoic deformation of the Kalpin fold-and-thrust belt, southern Chinese Tian Shan: New insights from low-T thermochronology and sandbox modeling. Tectonophysics 766, 416–432.

Chang, J., Qiu, N.S., 2017. Apatite low-temperature thermochronometry and applications to Tarim Basin in the Northwestern China. Earth Sci. Front. 24, 79–93 in Chinese with English abstract.

Chang, J., Qiu, N.S, Li, J.W, 2012. Tectono-thermal evolution of the northwestern edge of the Tarim Basin in China: Constraints from apatite (U-Th)/He thermochronology. J. Asian Earth Sci. 61, 187–198.

Chang, J., Qiu, N.S, Xu, W., 2017. Thermal regime of the Tarim Basin, Northwest China: a review. Int. Geol. Rev. 59 (1), 45–61.

Chang, J., Qiu, N.S, Zhao, X.Z, Shen, F.Y, Liu, N., Xu, W., 2018. Mesozoic and Cenozoic tectono-thermal reconstruction of the western Bohai Bay Basin (East China) with implications for hydrocarbon generation and migration. J. Asian Earth Sci. 160, 380–395.

Chen, H.H., Wu, Y., Feng, Y., Lu, Z.Y., Hu, S.Z., Yun, L., Qi, L.X., 2014. Timing and chronology of hydrocarbon charging in the Ordovician of Tahe oilfield, Tarim Basin, NW China. Oil Gas Geol. 35, 806–819 in Chinese with English abstract.

Chen, Q.L., Xi, B.B., Han, J., Xu, J., Wu, X., Zhu, X.X., Ma, Z.L., 2020. Preservation and influence factors of ultra-deep oil reservoirs in Shuntuoguole area, Tarim Basin: Evidence from fluid inclusions. China Petrol. Explor. 25, 121–133 in Chinese with English abstract.

Chen, R.Y., Zhao, W.Z., Wang, H.J., 2010. Fluid inclusion evidence for charge stages of hydrocarbon in the Ordovician traps of Tazhong area, Tarim Basin. Pet. Explor. Dev. 37, 537–542 in Chinese with English abstract.
Chen, Y.Q., Yan, W., Han, C.W., Yang, P.F., Li, Z., 2015. Redefinition on structural paleogeography and lithofacies paleogeography framework from Cambrian to Early Ordovician in the Tarim Basin: A new approach based on seismic stratigraphy evidence. Nat. Gas Geosci. 26, 1831–1843 in Chinese with English abstract.
Chi, G.X., Lu, H.Z., 2008. Validation and representation of fluid inclusion microthermometric data using the fluid inclusion assemblage (FIA) concept. Acta Petrologica Sinica 24, 1945–1953 in Chinese with English abstract.
Deng, S., Li, H.L., Zhang, Z.P., Wu, X., Zhang, J.B., 2018. Characteristics of differential activities in major strike-slip fault zones and their control on hydrocarbon enrichment in Shunbei area and its surroundings, Tarim Basin. Oil Gas Geol. 39, 878–888 in Chinese with English abstract.
Dyman, T.S., Crovelli, R.A., Bartberger, C.E., Takahashi, K.I., 2002. Worldwide estimates of deep natural gas resources based on the U.S. Geological Survey World Petroleum Assessment 2000. Nat. Resour. Res. 11, 207–218.
Fjeldskaar, W., Helset, H.M., Johansen, H., Grunnaleite, I., Horstad, I., 2008. Thermal modelling of magmatic intrusions in the Gjallar Ridge, Norwegian Sea: Implications for vitrinite reflectance and hydrocarbon maturation. Basin Res. 20 (1), 143–159.
Goldstein, R.H., Reynolds, T.J., 1994. Systematics of fluid inclusions in diagenetic minerals. SEPM Short Course 31, 199.
Gu, R., Yun, L., Zhu, X.X., Zhu, M., 2020a. Oil and gas sources in Shunbei Oilfield, Tarim Basin. Petrol. Geol. Exper. 42, 248-254+262 (in Chinese with English abstract).
Gu, Y., Huang, J.W., Jia, C.S., Shao, Z.B., Sun, T.G., Lu, Q.H., 2020b. Research progress on marine oil and gas accumulation in Tarim Basin. Petrol. Geol. Exper. 42, 1–12 in Chinese with English abstract.
Gu, Y., Wan, Y.L., Huang, J.W., Zhuang, X.B., Wang, B., Li, M., 2019. Prospects for ultra-deep oil and gas in the "deep burial and high pressure" Tarim Basin. Petrol. Geol. Exper. 41, 157–164 in Chinese with English abstract.
Guo, S., Hong, K., 2007. Silurian-Devonian sequence stratigraphy and favorable reservoir distribution in Tarim Basin. Acta Petrolei Sinica 28, 44–50 in Chinese with English abstract.
Han, Q., Yun, L., Jiang, H.S., Shao, X.M., Jin, X.M., 2021. Marine oil and gas filling and accumulation process in the north of Shuntuoguole Area in Northern Tarim Basin. J. Jilin Univ. (Earth Sci. Ed.) 51, 645–658 in Chinese with English abstract.
Hao, F., Sun, Y.C., Li, S.T., Zhang, Q.M., 1995. Overpressure retardation of organic-matter maturation and petroleum generation: A case study from the Yinggehai and Qiongdongnan Basins, South China Sea. AAPG Bull. 79, 551–562.
He, B.Z, Jiao, C.L, Xu, Z.Q, Cai, Z.H, Zhang, J.X, Liu, S.L, Li, H.B, Chen, W.W, Yu, Z.Y, 2016. The paleotectonic and paleogeography reconstructions of the Tarim Basin and its adjacent areas (NW China) during the late Early and Middle Paleozoic. Gondwana Res. 30, 191–206.
He, D.F., Jia, C.Z., Li, D.S., Zhang, C.J., Meng, Q.R., Shi, X., 2005. Formation and evolution of polycyclic superimposed Tarim Basin. Oil Gas Geol. 26, 64–77 in Chinese with English abstract.
Hu, J., Wang, T.G., Chen, J.P., Su, J., Cui, J.W., Zhang, B., Wang, X.M., 2015. Source recognition and charging analysis of oil in the Silurian bituminous sandstone in the Tarim Basin: Evidences from biomarker compounds. Nat. Gas Geosci. 26, 930–941 in Chinese with English abstract.
Jacob, H., 1989. Classification, structure, genesis and practical importance of natural solid oil bitumen. Int. J. Coal Geol. 11, 65–79.
Jia, C.Z., Pang, X.Q., 2015. Research processes and main development directions of deep hydrocarbon geological theories. Acta Petrolei Sinica 36, 1457–1469 in Chinese with English abstract.
Jiang, S., Zuo, Y.H, Yang, M.H, Feng, R.P, 2021. Reconstruction of the Cenozoic tectono-thermal history of the Dongpu Depression, Bohai Bay Basin, China: Constraints from apatite fission track and vitrinite reflectance data. J. Petrol. Sci. Eng. 205, 108809. https://doi.org/10.1016/j.petrol.2021.108809.
Jiao, F.Z., 2018. Significance and prospect of ultra-deep carbonate fault-karst reservoirs in Shunbei area, Tarim Basin. Oil Gas Geol. 39, 207–216 in Chinese with English abstract.
Jin, Z.J., 2011. Formation and accumulation of oil and gas in marine carbonate strata in Chinese sedimentary basins. Sci. China Earth Sci. 41, 910–926.
Kang, H.N., 2019. The Geochemical Characteristics and Accumulation Period of Oil and Gas in the north Shuntuoguole of Tarim Basin. China University of Petroleum-Beijing (in Chinese with English abstract).
Karlsen, D.A., Nedkvitne, T., Larter, S.R., Bjørlykke, K., 1993. Hydrocarbon composition of authigenic inclusions: Application to elucidation of petroleum reservoir filling history. Geochim. Cosmochim. Acta 57 (15), 3641–3659.
Li, H.L., Qiu, N.S., Jin, Z.J., 2005. Thermal history of central area of the Tarim Basin by apatite fission track analysis. Chin. J. Geol. 40, 129–132 in Chinese with English abstract.
Li, J.H., Zhou, X.B., Li, W.B., Wang, H.H., Liu, Z.L., Zhang, H.T., Ta, S.K., 2015. Preliminary reconstruction of tectonic paleogeography of Tarim Basin and its adjacent areas from Cambrian to Triassic, NW China. Geol. Rev. 61, 1225–1234 in Chinese with English abstract.
Li, M., Wang, T.-G., Lillis, P.G., Wang, C., Shi, S., 2012a. The significance of 24-norch-olestanes, triaromatic steroids and dinosteroids in oils and Cambrian-Ordovician source rocks from the cratonic region of the Tarim Basin, NW China. Appl. Geochem. 27 (8), 1643–1654.
Li, M., Wang, T., Chen, J., He, F., Yun, L.u., Akbar, S., Zhang, W., 2010a. Paleo-heat flow evolution of the Tabei uplift in Tarim Basin, northwest China. J. Asian Earth Sci. 37 (1), 52–66.
Li, S., Pang, X., Jin, Z., Yang, H., Xiao, Z., Gu, Q., Zhang, B., 2010b. Petroleum source in the Tazhong Uplift, Tarim Basin: New insights from geochemical and fluid inclusion data. Org Geochem. 41 (6), 531–553.
Li, Y., Xue, Z.J., Cheng, Z., Jiang, H.J., Wang, R.Y., 2020. Progress and development directions of deep oil and gas exploration and development in China. China Petrol. Explor. 25, 45–57. Chinese with English abstract.
Li, Y.-Q., Li, Z.-L., Sun, Y.-L., Santosh, M., Langmuir, C.H., Chen, H.-L., Yang, S.-F., Chen, Z.-X., Yu, X., 2012b. Platinum-group elements and geochemical characteristics of the Permian continental flood basalts in the Tarim Basin, northwest China: Implications for the evolution of the Tarim Large Igneous Province. Chem. Geol. 328, 278–289.
Li, Z.L, Chen, H.L, Song, B.A, Li, Y.Q, Yang, S.F, Yu, X., 2011. Temporal evolution of the Permian large igneous province in Tarim Basin in northwestern China. J. Asian Earth Sci. 42 (5), 917–927.
Li, Z.X., 2017. Analysis of Ordovician geochemical reservoir formation in Halahatang Xinken block. Southwest Petroleum University, Tarim Basin (in Chinese with English abstract).
Liang, Y.L., 2019. A research on hydrocarbon accumulation periods of the Cambrian in Tazhong area. Yangtze University (in Chinese with English abstract).
Lin, B., Zhang, X., Kuang, A.P., Yun, L., Liu, J., Li, Z.J., Cao, Z.C., Xu, X.C., Huang, C., 2021. Structural deformation characteristics of strike-slip faults in Tarim Basin and their hydrocarbon significance: A case study of No. 1 fault and No. 5 fault in Shunbei area. Acta Petrolei Sinica 42, 906–923 in Chinese with English abstract.
Lin, C.S, Yang, H.J, Liu, J.Y, Rui, Z.F, Cai, Z.Z, Zhu, Y.F, 2012. Distribution and erosion of the Paleozoic tectonic unconformities in the Tarim Basin, Northwest China: Significance for the evolution of paleo-uplifts and tectonic geography during deformation. J. Asian Earth Sci. 46, 1–19.
Liu, B.Z., 2020. Analysis of main controlling factors of oil and gas differential accumulation in Shunbei area, Tarim Basin-taking Shunbei No. 1 and No. 5 strike slip fault zones as examples. China Petrol. Explor. 25, 83–95 in Chinese with English abstract.
Liu, D.H., Shi, J.Y., 1994. Discussion on unconventional evaluation method of high evolution carbonate source rock. Pet. Explor. Dev. 21, 113–115 in Chinese.
Liu, S.W, Lei, X., Feng, C.G, Hao, C.Y, 2015. Estimation of subsurface formation temperature in the Tarim Basin, Northwest China: Implications for hydrocarbon generation and preservation. Int. J. Earth Sci. 105 (5), 1329–1351.
Liu, Y.C., Dong, S.Y., Zhao, C.H., 2021. Thermal evolution and the maturation of the deeply buried lower Paleozoic source rocks in the Tarim Basin, northwest China. Arabian J. Geosci. 14, 1238.
Liu, Y.C., Qiu, N.S., Chang, J., Jia, J.K., Li, H.L., Ma, A.L., 2020. Application of clumped isotope thermometry to thermal evolution of sedimentary basins: A case study of Shuntuoguole area in Tarim Bain. Geophys 63, 597–611 in Chinese with English abstract.
Lü, H.T., Geng, F., Mao, Q.Y., Wu, Q.Q., He, K., 2012. Favorable exploration targets in northern Avat and northern Shuntuoguole areas, Tarim Basin. Petrol. Geol. Explor. 34, 8–13 in Chinese with English abstract.
Lu, H.Z., Fan, H.R., Ni, P., Ou, G.X., Shen, K., Zhang, W.H., 2004. Fluid inclusions. Science Press.
Lu, X.S., Liu, K.Y., Zhao, M.J., Zhang, Y.Y., Lei, Y.L., Fan, J.J., Yu, Z.C., Zhuo, Q.G., Gui, L.Z., Li, X.L., 2017. Analytical techniques of geochronology and their applications in hydrocarbon accumulation research. Science Press.
Lu, Z.Y, Li, Y.T, Ye, N., Zhang, S.C, Lu, C.J, Li, W., Cheng, Z., Ding, X.Q, Zhu, B., Huang, B., Chen, S.N., 2020. Fluid inclusions record hydrocarbon charge history in the Shunbei Area, Tarim Basin, NW China. Geofluids 2020, 1–15.
Ma, Q.Y., Lü, H.T., Jiang, H.S., Li, X.Y., 2015. A division program of structural units in the Paleozoic platform-basin region, Tarim Basin. Marine Origin Petrol. Geol. 20, 1–9 in Chinese with English abstract.
McTavish, R.A., 1998. The role of overpressure in the retardation of organic matter maturation. J. Pet. Geol 21 (2), 153–186.
Mu, Z.H., Tang, Y., Cui, B.F., Xiao, Y.J., Wang, G.L., 2002. Erosion thickness restoration in southwest Tarim Basin. Acta Petrolei Sinica 23, 40–44 in Chinese with English abstract.
Ni, Z.Y., Wang, T.G., Li, M.J., Fang, R.H., Li, Q.M., Tao, X.W., Cao, W., 2016. An examination of the fluid inclusions of the Well RP3-1 at the Halahatang Sag in Tarim Basin, northwest China: Implications for hydrocarbon charging time and fluid evolution. J. Petrol. Sci. Eng. 146, 326–339.
Qi, L.X., 2016. Oil and gas breakthrough in ultra-deep Ordovician carbonate formations in Shuntuoguole uplift, Tarim Basin. China Petrol. Explor. 21, 38–51 in Chinese with English abstract.
Qi, L.X., 2020. Characteristics and inspiration of ultra-deep fault-karst reservoir in the Shunbei area of the Tarim Basin. China Petrol. Explor. 25, 102–111 in Chinese with English abstract.
Qi, Y.A., Liu, G.C., 1999. Wave process analysis of sedimentary basin and erosion quantity of unconformities. J. Jiaozuo Inst. Technol. 18, 8–12.
Qiu, N.S, Chang, J., Zuo, Y.H, Wang, J.Y, Li, H.L, 2012. Thermal evolution and maturation of lower Paleozoic source rocks in the Tarim Basin, northwest China. AAPG Bull. 96 (5), 789–821.
Qiu, N.S, Jiang, G., Mei, Q.H, Chang, J., Wang, S.J, Wang, J.Y, 2011. The Paleozoic tectonothermal evolution of the Bachu Uplift of the Tarim Basin, NW China: Constraints from (U-Th)/He ages, apatite fission track and vitrinite reflectance data. J. Asian Earth Sci. 41 (6), 551–563.
Qiu, N.S., Wang, J.Y., Mei, Q.H., Jiang, G., Tao, C., 2010. Constraints of (U-Th)/He ages on early Paleozoic tectonothermal evolution of the Tarim Basin, China. Sci China Earth Sci 53 (7), 964–976.

Randive, K.R., Hari, K.R., Dora, M.L., Malpe, D.B., Bhondwe, A.A., 2014. Study of fluid inclusions: Methods, techniques and applications. Gondwana Geol. Magaz. 29, 19–28.
Ren, Z.L., Cui, J.P., Qi, K., Yang, G.L., Chen, Z.J., Yang, P., Wang, K., 2020. Control effects of temperature and thermal evolution history of deep and ultra-deep layers on hydrocarbon phase state and hydrocarbon generation history. Nat. Gas. Ind. 40, 22–30 in Chinese with English abstract.
Shi, W.J., Jiang, H., Xi, B.B., 2012. Application of the PVTX simulation of reservoir fluid inclusions to estimate petroleum charge stages: A case study in the Tuoputai Area of Tarim Basin. Geol. J. China Universities 18, 125–132 in Chinese with English abstract.
Si, S.H., Chen, H.H., Tan, X.F., Li, C.Q., Wu, Y., Li, N., 2013. Hydrocarbon accumulation period and its carrier systems in Ordovician reservoir of Yubei Area, Markit Slope Tarim Basin. Earth Sci. 38, 1271–1280 in Chinese with English abstract.
Sun, L.F, Zou, C.N, Zhu, R.K, Zhang, Y.H, Zhang, S.C, Zhang, B.M, Zhu, G.Y, Gao, Z.Y, 2013. Formation, distribution and potential of deep hydrocarbon resources in China. Pet. Explor. Dev. 40 (6), 687–695.
Sweeney, J., Burnham, A., 1990. Evaluation of a simple model of vitrinite reflectance based on chemical kinetics. AAPG Bull. 74, 1559–1570.
Tissot, B.P., Welte, D.H., 1978. Petroleum formation and occurrence: A new approach to oil and gas exploration. Springer-Verlag, Heidelberg, New York, Berlin, p. p538.
Wang, B., Feng, Y., Zhao, Y.Q., Zhou, Y.S., Luo, Y., Zhang, G.F., 2015. Determination of hydrocarbon charging history by diagenetic sequence and fluid inclusions: a case study of the Kongquehe area in the Tarim Basin. Acta Geologica Sinica (English Edition) 89 (3), 876–886.
Wang, B., Zhao, Y.Q., He, S., Guo, X.W., Cao, Z.C., Deng, S., Wu, X., Yang, Y., 2020. Hydrocarbon accumulation stages and their controlling factors in the northern Ordovician Shunbei 5 fault zone, Tarim Basin. Oil & Gas Geol. 41, 965–974. Chinese with English abstract.
Wang, J.B., Guo, R.T., Xiao, X.M., Liu, Z.F., Shen, J.G., 2002. Timing and phases of hydrocarbon migration and accumulation of the formation of oil and gas pools in Lunnan Low Uplift of Tarim Basin. Acta Sedimentol. Sin. 20, 320–325 in Chinese with English abstract.
Wang, K., Lu, X.C, Chen, M., Ma, Y.M, Liu, K.Y, Liu, L.Q, Li, X.Z, Hu, W.X, 2011. Numerical modelling of the hydrocarbon generation of Tertiary source rocks intruded by doleritic sills in the Zhanhua depression, Bohai Bay Basin, China. Basin Res. 24 (2), 234–247.
Wang, L.S., Li, C., Yang, C., 1996. The lithospheric thermal structure beneath Tarim Basin, western China. Chin. J. Geophys. 39, 794–803 in Chinese with English abstract.
Wang, Y.W., 2019. Multiple original mechanisms of the Ordovician reservoir and their control on hydrocarbon charging in Shuntuoguole area. China University of Geosciences-Wuhan, Tarim Basin (in Chinese with English abstract).
Wang, Y.W., Chen, H.H., Guo, H.F., Zhu, Z.H., Wang, Q.R., Yu, P., Qi, L.X., Yun, L., 2019. Hydrocarbon charging history of the ultra-deep reservoir in Shun 1 strike-slip fault zone, Tarim Basin. Oil Gas Geol. 40, 972–989 in Chinese with English abstract.
Wu, G.H., Deng, W., Huang, S.Y., Zheng, D.M., Pan, W.Q., 2020. Tectonic-paleogeographic evolution in the Tarim Basin. Chin. J. Geol. 55, 305–321 in Chinese with English abstract.
Wu, X., Li, D., Han, J., Zhu, X.X., Huang, C., Cao, Z.C., Chang, J., Liu, Y.C., 2022. Characteristics of present ultra-deep geothermal field in the northern Shuntuoguole low uplift, Tarim Basin. Acta Petrolei Sinica 43, 29–40. Chinese with English abstract.
Wu, X.L., Li, R.X., Li, C.Q., Si, S.H., Li, D.L., Zhao, B.S., Cheng, J.H., Wang, J.G., Qiao, B., 2017. Characteristics of fluid inclusions and hydrocarbon accumulation history in Ordovician reservoir of Yubei area, Tarim Basin. J. Lanzhou Univ. (Nat. Sci.) 53, 740–748 in Chinese with English abstract.
Wu, Y.D., Zhang, Z.N., Ji, L.M., Sun, L.N., He, C., Su, L., Xia, Y.Q., 2016. The changes of hydrocarbon yield and Ro for source rock in the semi-open simulation with increasing of fluids pressure. Nat. Gas Geosci. 27, 883–891 in Chinese with English abstract.
Xing, Y.L., Zhang, N., Zhang, B.S., Zhao, R.H., Chen, Y.G., Yang, X.G., 2011. Characteristics of hydrocarbon inclusions and the timing of the hydrocarbon accumulation in the Lianglitage Fm in Tazhong 26–24 well block. Oil Gas Geol. 32, 651–658 in Chinese with English abstract.
Xiong, L.P., Gao, W.A., 1982. Characteristics of geotherm in uplift and depression. Chin. J. Geophys. 25, 60–68 in Chinese with English abstract.
Xu, Y.G., Wei, X., Luo, Z.Y., Liu, H.Q., Cao, J., 2014. The Early Permian Tarim large igneous province: Main characteristics and a plume incubation model. Lithos 204, 20–35.
Yang, F.L., Wang, T.G., Li, M.J., 2016. Geochemical study of Cambrian source rocks in the cratonic area of Tarim Basin, NW China. Nat. Gas Geosci. 27, 861–872.
Yang, H.J., Chen, Y.Q., Tian, J., Du, J.H., Zhu, Y.F., Li, H.H., Pan, W.Q., Yang, P.F., Li, Y., An, H.T., 2020. Great discovery and its significance of ultra-deep oil and gas exploration in Well Luntan-1 of the Tarim Basin. China Petrol. Explor. 25, 62–72 (in Chinese with English abstract).
Yang, S.F., Chen, H.L., Li, Z.L., Li, Y.Q., Yu, X., Li, D.X., Meng, L.F., 2014. Early Permian Tarim large igneous province in northwest China. Sci. China: Earth Sci. 56 (12), 2015–2026.
Yang, Y.J., Liu, J.D., Tian, J.C., Meng, W.B., Zhang, X., Zhu, H., 2011. Sequence lithofacies paleogeography of Cambrian in Tarim Basin. Nat. Gas Geosci. 22, 450–459.
Yu, S., Pan, C., Wang, J.J, Jin, X.D, Jiang, L.L, Liu, D.Y, Lü, X.X, Qin, J.Z, Qian, Y.X, Ding, Y., Chen, H.H, 2011. Molecular correlation of crude oils and oil components from reservoir rocks in the Tazhong and Tabei Uplifts of the Tarim Basin, China. Organ Geochem. 42 (10), 1241–1262.
Zhang, C.L., Zou, H.B., Li, H.K., Wang, H.Y., 2013. Tectonic framework and evolution of the Tarim Block in NW China. Gondwana Res. 23 (4), 1306–1315.
Zhang, G.Y., Zhao, W.Z., Wang, H.J., Li, H.H., Liu, L., 2007. Multicycle tectonic evolution and composite petroleum systems in the Tarim Basin. Oil Gas Geol. 28, 653–663 in Chinese with English abstract.
Zhang, J.F., 2016. Reservoir geochemical study of Katake Uplift and adjacent area in Tarim Basin. China University of Petroleum-Beijing (in Chinese with English abstract).
Zhang, S.C., Hanson, A.D., Moldowan, J.M., Graham, S.A., Liang, D.G., Chang, E., Fago, F., 2000. Paleozoic oil-source rock correlations in the Tarim Basin, NW China. Org Geochem. 31 (4), 273–286.
Zhang, S.C, Huang, H.P, 2005. Geochemistry of Palaeozoic marine petroleum from the Tarim Basin, NW China: Part 1. oil family classification. Org Geochem. 36 (8), 1204–1214.
Zhang, S.C., Liang, D.G., Li, M.W., 2002. Correlation between molecular fossils and oil sources in Tarim Basin. Chin. Sci. Bull. 47, 16–23 in Chinese with English abstract.
Zhang, S.C., Zhang, B.M., Li, B.L., Zhu, G.Y., Su, J., Wang, X.M., 2011. History of hydrocarbon accumulations spanning important tectonic phases in marine sedimentary basins of China: Taking the Tarim Basin as an example. Pet. Explor. Dev. 38 (1), 1–15.
Zhang, X., Tian, J.C., Peng, J., 2008. The lithofacies-paleogeography and space-time evolvement of Silurian-Devonian in the Tarim Basin. Acta Sedimentol. Sin. 26, 762–771 in Chinese with English abstract.
Zhang, Y.M., 2021. Petroleum charge history of the slope area of Katake Uplift in Tarim Basin. Petrol. Geol. Exper. 43, 1015–1023 in Chinese with English abstract.
Zhao, R.H., Zhang, N., Xing, Y.L., Chen, Y.G., 2011. Analysis on Ordovician hydrocarbon accumulation stages in well block Tazhong 45. J. Oil Gas Technol. 33, 30-34+5 (in Chinese with English abstract).
Zhu, G., Milkov, A.V., Zhang, Z.Y, Sun, C.H, Zhou, X.X, Chen, F., Han, J.F, Zhu, Y., 2019. Formation and preservation of a giant petroleum accumulation in superdeep carbonate reservoirs in the southern Halahatang oil field area, Tarim Basin, China. AAPG Bull. 103 (7), 1703–1743.
Zhu, G.Y., Cao, Y.H., Yan, L., Yang, H.J., Sun, C.H., Zhang, Z.Y., Li, T.T., Chen, Y.Q., 2018. Petroleum exploration potential and favorable areas of ultra-deep marine strata deeper than 8,000 meters in Tarim Basin. Nat. Gas Geosci. 29, 755–772 in Chinese with English abstract.
Zhu, G.Y., Jin, Z.J., Hu, W.X., Zhang, X.F., Yao, S.P., 2007. Comparative study of free hydrocarbons in pores with inclusion hydrocarbons and oil-source rock correlation for Silurian sandstone in Tazhong area. Oil Gas Geol. 28, 25–34 in Chinese with English abstract.
Zhu, G.Y., Zhang, S.C., Zhang, B., Su, J., Yang, D.B., 2010. Reservoir types of marine carbonates and their accumulation model in western and central China. Acta Petrolei Sinica 31, 871–878 in Chinese with English abstract.
Zhu, X.X., Chen, X.Y., Cao, Z.C., 2017. Hydrocarbon accumulation mode of Shuntuo 1 well block in the Shuntuoguole lower uplift, Tarim Basin. Petrol. Geol. Exper. 39, 41–49 in Chinese with English abstract.